ISSN 0304-3851

PUBLISHED QUARTERLY VOL. 2, NO. 2, JUNE 1977

JOURNAL OF APPLIED SCIENCE AND ENGINEERING

SECTION A ELECTRICAL POWER AND INFORMATION SYSTEMS

ELSEVIER SCIENTIFIC PUBLISHING COMPANY AMSTERDAM
& NORTH HOLLAND PUBLISHING COMPANY AMSTERDAM

JOURNAL OF APPLIED SCIENCE AND ENGINEERING
SECTION A: ELECTRICAL POWER AND INFORMATION SYSTEMS

Published under the aegis of
Royal Institution of Engineers in the Netherlands (K.I.v.I.)
Netherlands Electronic and Radio Institution (N.E.R.G.)

The aim of the journal is to encourage the interchange of ideas on electrical engineering and its associated theories. Only original papers of high academic quality will be considered; they may be theoretical, experimental or practical. Emphasis will be placed on work that elucidates understanding of the basic theories used in electrical engineering and, where possible, provides information of value to the practising engineer.

Journal of Applied Science and Engineering (JASE), Section A: Electrical Power and Information Systems, will publish work in the fields of electrical power generation and distribution, electrical machinery, cables, high-voltage and switching phenomena, telecommunication in all its aspects, electronics, micro-electronics, systems engineering, analog and digital computers and the materials used in ali of them.

Journal of Applied Science and Engineering A, 2 (1977) 77 - 90

SYNCHRONOUS MACHINE PERFORMAXCE IMPROVEMENT WITH DECOUPLED ACTIVE AND REACTIVE POWER CONTROL LOOPS

K. RAJA REDDY and M.P. DAVE

Department of Electrical Engineering, University of Roorkec, Roorkee (India)

(Received December *24*, 1975)

Summary

The synchronous machine-infinite bus system can be regarded as a multi-input-multi-output control system with the control inputs as changes in excitations and prime mover inpute and the outputs as reactive and active powers. In general there exists considerable coupling between the inputs and outputs. The decoupling of ''P and &'' control loops not only improves the performance of the system but also simplifies the controller design since the difficulty of design is closely associated with the degree of coupling between the various control loops.

In the present paper the decoupling of active and reactive power control loops is achieved by state feedback with measurable states. First, small signal operation (dynamic) is studied to determine F and G matrices to decouple the two control loops. The state feedback used for decoupling is also utilized to locate most of the closed loop poles at the desired places. The next part of the paper covers the transient stability analysis of the decoupled system. It is shown that decoupling of power control loops improves the dynamic and transient performance of the system.

1. Introduction

The problem of the decoupling of a time invariant linear system by state feedback was first considered by Morgan [1]. The necessary and sufficient conditions for decoupling were proposed by Falb and Wolovich [2]. The decoupling technique has been applied to flight control and chemical process control and it is seeking application to power system problems. Nolan et al. [3] have applied the decoupling technique to the optimization of turbo-

alternator dynamic response. We [4] have applied this technique to decouple the two control loops of active and reactive power of a turbogenerator-infinite bus system (under dynamic conditions) without governor and voltage regulator.

The main difficulty in designing controllers by state feedback is that the state variables used are not directly measurable. Of course Luenberger's [5] observer can be constructed to estimate the unmeasurable states from the information available. But the addition of a dynamic observer will make the overall controlled system more complex and unduly sensitive to disturbances and changes in parameters [6]. Generally the machine equations contain flux linkages as state variables which are not measurable. These flux linkages can be expressed in terms of measurable quantities by a linear transformation [7]. In the first part of this paper the active and reactive power control loops of a turbogenerator-infinite bus system with regulator and governor are decoupled, under dynamic conditions, by measurable state feedback.

Good transient response can only be obtained if at least part of the response occurs very quickly by the direct control of steam flow at a point close to the turbine. Morgan et al. [8] and Cushing et al. [9] have applied the turbine fast valving to improve the transient stability. Dandeno et al. [10] have found that superposition of supplementary signals on the error signal to the voltage regulator will improve system stability limits. The feedback used for decoupling provides additional signals which are used to control the voltage regulator and HP turbine inlet vlaves to improve the transient stability of the system.

The transient stability studies are also made for the following cases to enable direct comparison to be made with the transient response of the decoupled system.

(1) The fast intercepter valving

(2) Combination of (1) and the feedback signals controlling voltage regulator and HP turbine inlet valves.

(3) With conventional excitation control and governor.

The swing curves for the above cases are drawn for different reactive power loadings. It has been found that the state feedback used for decoupling improves both dynamic and transient performance of the system over a fairly wide range of operating conditions.

2. System model

The system shown in Fig. 1 consists of a turbogenerator connected to an infinite bus through double circuit line. The generator is fitted with an automatic voltage regulator with derivative stabilizing circuit. The steam turbine (Fig. 2) is represented by one time constant. The system is represented by the machine performance eyns. (A1)—(A3) [11] given in Appendix A and

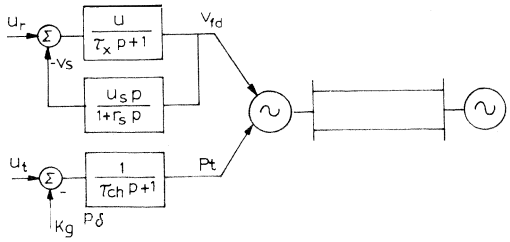

Fig. 1. System model.

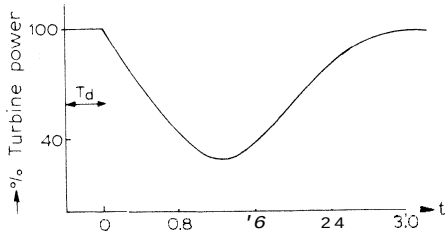

Fig. 2. Turbine power response.

the following expressions for Q and P, voltage regulator and governor respectively.

$$Q = v_q i_d - v_d i_a \tag{1}$$

$$P = v_q i_q + v_d i_d \tag{2}$$

$$v_{fd} = \frac{\mu}{1 + \tau_x p}(u_r - v_s) \tag{3}$$

$$v_s = \frac{1}{1 + \tau_s p} v_{fd} \tag{4}$$

$$P_t = \frac{1}{1 + \tau_{ch} p}(u_t - k_g p\delta) \tag{5}$$

3. Dynamic analysis

If a Taylor series expansion is taken for the eqns. (A1)—(A3) and (1)—(5) about an operating point, the resulting linear perturbation model can be represented in state space form as

$$\left.\begin{aligned} \dot{\boldsymbol{x}} &= A\boldsymbol{x} + B\boldsymbol{u} \\ \boldsymbol{y} &= C\boldsymbol{x} \end{aligned}\right\} \tag{6}$$

where

$\boldsymbol{x} = [\Delta\delta, \Delta\dot{\delta}, \Delta\phi_{fd}, \Delta v_{fd}, \Delta v_s, \Delta P_t]^t$

$\boldsymbol{u} = [\Delta u_r, \Delta u_t]^t$

$\boldsymbol{y} = [\Delta Q, \Delta P]^t$

A, B and *C* are constant real matrices.

The state vector x contains d-axis field flux linkage $\Delta\phi_{fd}$ which is unmeasurable. $\Delta\phi_{fd}$ can be expressed in terms of the field current which is measurable. Therefore we can find a non-singular matrix M [7] which relates the new state vector $\boldsymbol{z}$ containing all measurable states to the state vector $\boldsymbol{x}$ by the equation:

$\boldsymbol{z} = M\boldsymbol{x}$

where

$z = [\Delta\delta, \Delta\dot{\delta}, \Delta i_{fd}, \Delta v_{fd}, \Delta v_s, \mathrm{AP},]^t$

Then

$\dot{z} = M\dot{x} \pm MAM^{-1}z + MBu = \overline{A}z + \overline{B}u$

$y = Cx = CM^{-1}z = \overline{C}z$

where

$$\overline{A} = MAM^{-1},\ \overline{B} = MB,\ \overline{C} = CM^{-1} \qquad (7)$$

The computation of matrix M is given in Appendix B. The constant matrices $\overline{A}$, B and $\overline{C}$ of the system are given by

$$\overline{A} = \begin{bmatrix} 0 & 1 & 0 & 0 & 0 & 0 \\ a_{21} & a_{22} & a_{23} & 0 & 0 & \frac{1}{\overline{M}} \\ a_{31} & a_{32} & a_{33} & a_{34} & 0 & 0 \\ 0 & 0 & 0 & -\frac{1}{\tau_x} & -\frac{\mu}{\tau_x} & 0 \\ 0 & 0 & 0 & a_{54} & a_{55} & 0 \\ 0 & -\frac{k_g}{\tau_{ch}} & 0 & 0 & 0 & -\frac{1}{\tau_{ch}} \end{bmatrix}, B = \begin{bmatrix} 0 & 0 \\ 0 & 0 \\ 0 & 0 \\ \frac{\mu}{\tau_x} & 0 \\ b_{51} & 0 \\ 0 & \frac{1}{\tau_{ch}} \end{bmatrix},$$

$$\overline{C} = \begin{bmatrix} C_{11} & 0 & C_{13} & 0 & 0 & 0 \\ C_{21} & 0 & C_{23} & 0 & 0 & 0 \end{bmatrix}$$

The expressions for the elements of $\overline{A}$ and $\overline{C}$ matrices are given in Appendix C.

4. Decoupling of multivariable control systems

Consider a linear time invariant dynamical system S defined by state space equations:

$$\dot{\boldsymbol{x}} = A\boldsymbol{x} + B\boldsymbol{u}$$
$$\boldsymbol{y} = C\boldsymbol{x} \tag{9}$$

where $\boldsymbol{x}$ is an n-state vector, $\boldsymbol{u}$ is an m-input vector, $\boldsymbol{y}$ is an m-output vector and A, B, C are constant matrices. The system S is said to be decoupled by a control law

$$\boldsymbol{u} = F\boldsymbol{x} + G\boldsymbol{v} \tag{10}$$

if the B^* matrix is non-singular [2].

Where v is a new input vector, F and G are m X n and m X m constant matrices and

$$B^* = [C_i A^{d_i} B], \quad i = 1, 2, \ldots, m \tag{11}$$

$$d_i = \min j: C_i A^j B \neq 0, \; j = 0, 1, \ldots, n-1$$
$$= n - 1 \text{ if } C_i A^j B = 0 \text{ for all values of } j$$

C_i is the i-th row of C

Then the G and F matrices are given by

$$G = B^{*-1} \tag{12}$$

$$F = B^{*-1}\left[\sum_{k=0}^{d} M_k C A^k - A^*\right] \tag{13}$$

where $d = \max d_i$, M_k, k = 0, 1, ..., d are m X m diagonal matrices and A' = $[C_i A^{d_i+1}]$, i = 1, 2, ..., m.

The above feedback matrix F includes the location of $m + d_1 + d_2 + \ldots d_m$ closed loop poles at the desired places.

If the B^* matrix is singular then the system can be decoupled by insertion of a precompensator at the input terminals [12].

5. Transient stability analysis of the decoupled system

The transient stability of the system can be improved by employing special signals to control the voltage regulator and the steam turbine valves. The state feedback used for decoupling provides such special signals which are shown to improve the stability.

The state feedback decoupling arrangement of the system is shown in Fig. 3. For the transient analysis we assume that the new input vector v will remain at its value just before the occurrence of the disturbance. The two

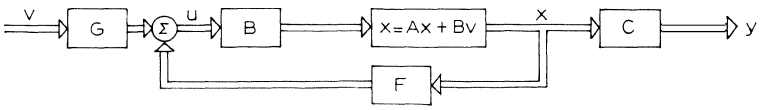

Fig. 3. State feedback decoupling arrangement.

inputs $\bar{u}_1$, $\bar{u}_2$ ($\bar{u} = F\bar{x}$) available due to feedback are used to control the voltage regulator and HP turbine steam inlet valves. Realistic restrictions are imposed on (1) maximum and minimum values of field voltage and turbine output and (2) rate of increase and decrease of turbine power.

For transient stability analysis of the decoupled system the following differential and network equations are to be solved simultaneously.

$$\mathrm{p}(\delta) = \mathrm{p}\delta \tag{14}$$

$$\mathrm{p}(\mathrm{p}\delta) = \frac{1}{M}[P - P_u - D(\mathrm{p}\delta) + \Delta P_t] \tag{15}$$

$$\mathrm{p}(i_{fd}) = \frac{x_d + x_e}{x'_d + x_e} \cdot \frac{1}{\tau_f}(v_{fd} - i_{fd}) + \frac{V_b \sin \delta}{x'_d + x_e}(x_d - x'_d)\,\mathrm{p}\delta \tag{16}$$

$$\mathrm{p}(v_{fd}) = \frac{1}{\tau_x}[-v_{fd} + \mu(V_r - v_t - v_s + u_1)] \tag{17}$$

$$\mathrm{p}(v_s) = \frac{1}{\tau_s}[-v_s + \mu_s(\mathrm{p}v_{fd})] \tag{18}$$

$$\mathrm{p}(\Delta \mathrm{p}_t) = \frac{1}{\tau_{ch}}[-k_g(\mathrm{p}\delta) - \Delta P_t + \bar{u}_2] \tag{19}$$

$$i_d = \frac{i_{fd} - V_b \cos \delta}{x_d + x_e} \tag{20}$$

$$i_q = \frac{V_b \sin \delta}{x_q + x_e} \tag{21}$$

$$v_d = V_b \sin \delta - x_e i_q \tag{22}$$

$$v_q = V_b \cos \delta + x_e i_d \tag{23}$$

$$v_t^2 = v_q^2 + v_d^2 \tag{24}$$

$$P_u = v_q i_q + v_d i_d \tag{25}$$

6. Numerical example

The procedure and results are illustrated with the help of the following example. The parameters of the system and the initial operating conditions

at the nominal operating point (0.9 pf lag) are given below [11,13].

$V_t = 1, P = 0.8, M = 0.0337, D = 0.00945, \mu = 20, \mu_s = 0.014, k_g = 0.05, x_d = 2, x_d' = 0.232, x_q = 1.7, x_e = 0.18, V_b = 0.9414, \delta = 48.2^0$, $\iota_{fd} = \upsilon_{fd} = 2.387, \tau_f = 6$ s, $\tau_x = 0.2$ s, $\tau_s = 2$ s and $\tau_{ch} = 0.5$ s.

6.1 Dyanmic decoupling

The $\bar{A}$, $\bar{B}$, $\bar{C}$ matrices of eyn. (8)are calculated for the nominal operating point. Since the B^* matrix calculated using eqn. (11) is singular a precompensator is required for decoupling the system. The first order precompensator [12] has the following state space form:

$$\hat{A} = [0], \hat{B} = [r_1 \quad 0], \hat{C} = \begin{bmatrix} r_2 \\ 0 \end{bmatrix}, \hat{D} = \begin{bmatrix} 0 & 0 \\ r_3 & r_4 \end{bmatrix}$$

The new state vector x and the matrices $\underline{A}, \underline{B}$ and $\underline{C}$ for the composite system are given by

$$\underline{A} = \begin{bmatrix} \bar{A} & \bar{B}\hat{C} \\ 0 & \hat{A} \end{bmatrix}, \underline{B} = \begin{bmatrix} \bar{B}\hat{D} \\ \hat{B} \end{bmatrix}, \underline{C} = [\bar{C} \quad 0], \underline{x} = \begin{bmatrix} x \\ z \end{bmatrix} \tag{26}$$

For the above composite system with $r_2 = r_3 = 1$ and $r_1 = r_4 = 2$, we have $d_1 = d_2 = 2$ and B^* matrix nonsingular. Hence the system with the precompensator eyn. (26) is decoupled by control law eyn. (10). Since $m + d_1 + d_2 = 6$, only 6 poles out of 7 can be placed at desired locations. The F and G matrices with the poles located at $-3, -10 \pm j4, -4$, and $-2 \pm j8$, are calculated using eqns. (13) and (12) as

$$F = \begin{bmatrix} 8.498 & -0.511 & 0.162 & -0.378 & 10.67 & -4.24 & -10.92 \\ -6.43 & 0.18 & 0.044 & 0.267 & -8.3 & 2.05 & 8.42 \end{bmatrix} \tag{27}$$

$$G = \begin{bmatrix} 0.0183 & -0.00638 \\ -0.014 & 0.0101 \end{bmatrix}$$

The decoupled system will have the following closed loop transfer function

$$H(s) = \begin{bmatrix} 1/(s+3)(s^2 + 20s + 116) & 0 \\ 0 & 1/(s+4)(s^2 + 4s + 68) \end{bmatrix} \tag{28}$$

The seventh closed loop pole which is not affected by state feedback is located at -0.5.

To investigate the sensitivity of the decoupled system against changes in operating point, closed loop transfer functions at two operating points (upf and 0.8 pf lag) are computed using F and G matrices of eqn. (27).

The unit step responses of the elements of transfer function $H(s)$ (h_{11}, h_{12}, h_{21}, h_{22}) at operating points 0.9 pf lag, upf, and 0.8 pf lag are shown in Fig. 4. The corresponding step responses for the original system are given in Fig. 5. It can be seen from the time responses that the strong coupling term

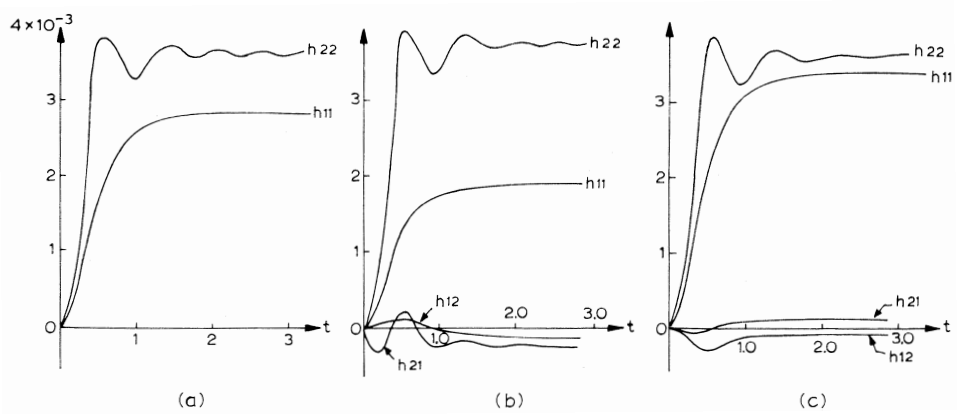

Fig. 4. Unit step response of the decoupled system. (a) 0.9 pf lagging; (b) Unity power factor; (c) 0.8 pf lagging.

h_{12} of the natural system is reduced to zero at 0.9 pf lag (complete decoupling) and to a very small value at other operating points.

6.2 Transient stability analysis

The transient stability studies are made for a 3-phase fault at the sending end of the transmission line. The fault is assumed to be cleared with the disconnection of the faulty line by simultaneous operation of circuit breakers at either end.

Due to the precompensator, we get one more differential equation:

$$p(z) = r_1 v_1 \tag{29}$$

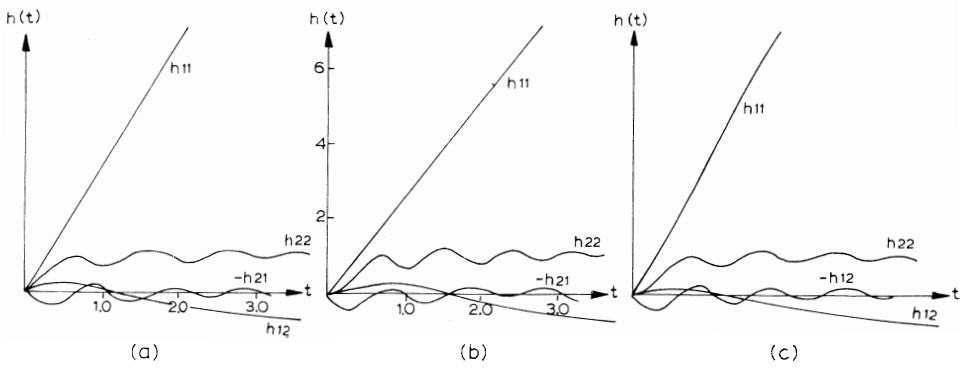

Fig. 5. Unit step response of the natural system. (a) 0.9 pf lagging; (b) Unity power factor; (c) 0.8 pf lagging.

The additional inputs due to feedback are given by

$\overline{u}_1 = r_2 z$

$\overline{u}_2 = r_3 v_1 + r_4 v_2$, where $v = F\underline{x}$

For transient stability studies, the 7 differential eqns. (14)—(19)and (29)

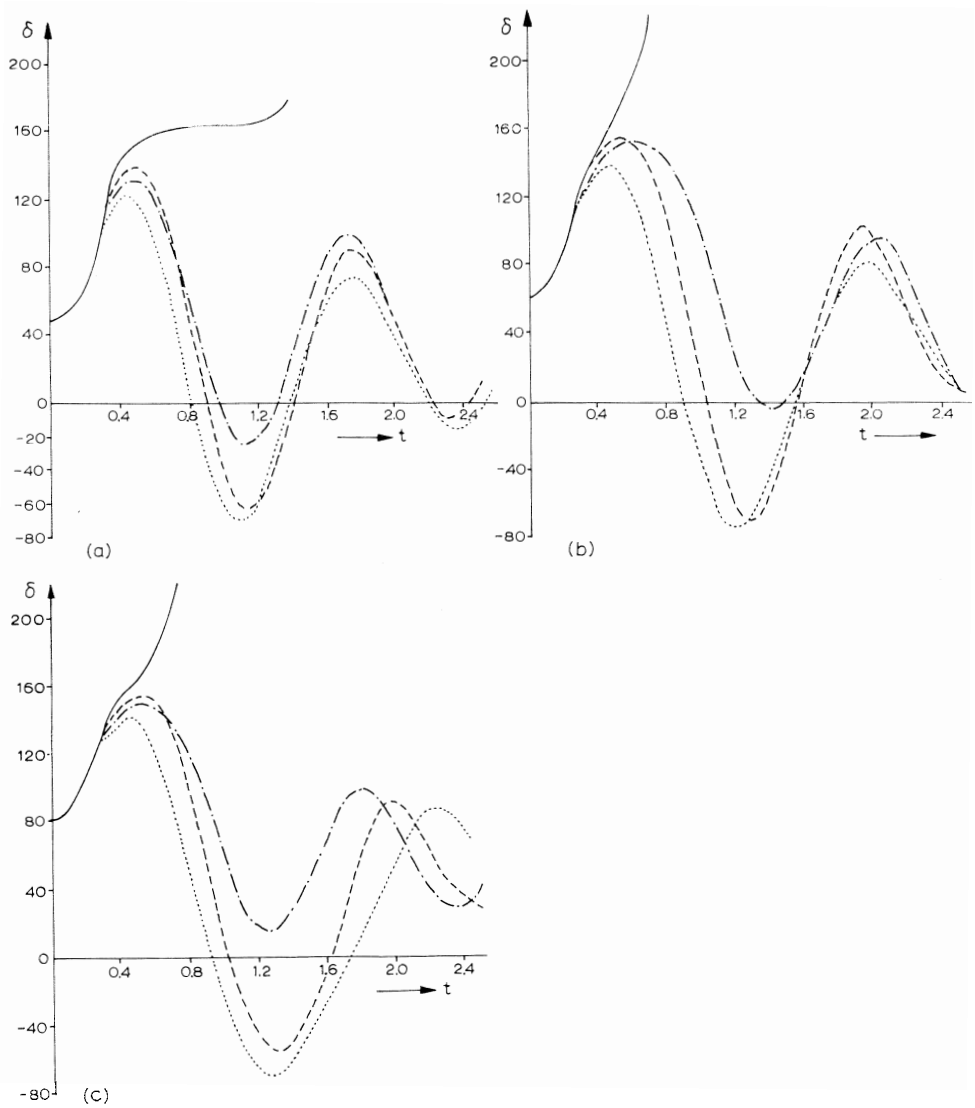

Fig. 6 Swing curves. (a) 0.9 pf lagging with FCT = 0.3 s. (b) Unity power factor with FCT = 0.29 s. (c) 0.9 pf leading with FCT = 0.23 s. ——— Natural system; - . - . - . - decoupled system; - - - - - - Fast turbine valving; . . . . . Combination of fast turbine valving and feedback used for decoupling (This notation applies to Fig. 7 also).

together with network eqns. (20)—(25) are solved simultaneously using the Runge—Kutta—Gill method [14] with a time step of 0.01 s.

The swing curves are drawn for the following cases with $v_{fdmax} = 6.12$ pu and $v_{fdmin} = 0$.

(1) Additional inputs due to feedback controlling voltage regulator and HP turbine inlet valves with the following restrictions: $P_{tmax} = 0.8$ pu, $P_{tmin} = 0.56$ pu (it is assumed that the HP turbine controls 30% of the total turbine output), turbine power rate of decrease = 1 pu/s and rate of increase = 0.1 pu/s [13].

(2) Turbine fast valving using turbine power response as shown [8] in Fig. 2 with $T_d = 0.1$ s.

(3) Combination of (1) and (2)

(4) Using conventional excitation control and governor.

To investigate the effect of changes in the initial operating conditions on the transient stability, the swing curves for the above 4 cases are drawn (Fig. 6) for the following reactive power loadings with P = 0.8 pu.

(a) Nominal operating point 0.9 pf lagging (Q = 0.3855 pu) with FCT = 0.3 s.

(b) Unity power factor (Q = 0) with FCT = 0.29 s.

(c) 0.9 pf leading (Q = —0.3855 pu) with FCT = 0.23 s.

The terminal voltage recovery curves at the nominal operating point (0.9 pf lag) for the above 4 cases are shown in Fig. 7.

It is observed from Fig. 6 that the natural system, which is unstable, is made stable by the additional signals due to feedback controlling the voltage regulator and the HP turbine inlet valves. It can be seen from the swing curves that the maximum rotor angle δ during first forward and backward swing is less for the decoupled system than the fast turbine valving. Greater

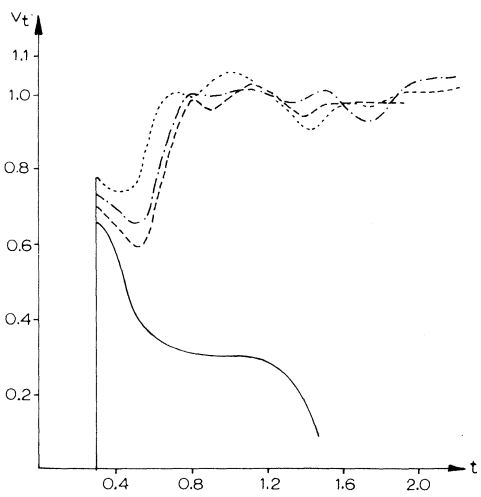

Fig. 7. Terminal voltage recovery curves at 0.9 pf lagging.

improvement in stability limit can be obtained by the combination of the fast valving and the feedback for decoupling. This is expected because the combination makes it possible to bring the entire output of the turbine under the control of supplementary signals. From Fig. 7, it can be seen that the voltage recovery curve for the decoupled system is better than for the other cases.

7. Conclusions

Under dynamic conditions, the state feedback used for decoupling the control loops of active and reactive power helps in reducing the coupling present between the two control loops to zero at the nominal operating point and to a very small value at other operating points. The state feedback also helps in locating most of the closed loop poles at the desired locations.

Under the transient conditions, the feedback used for decoupling provides additional signals which improve the stability over a fairly wide range of initial operating conditions. The relative improvement in the stability limit will depend upon (1) the rate of increase and decrease of turbine power, (2) the upper and lower limits of turbine power, and (3) the feedback matrix F. The transient analysis conducted also revealed that greater improvement in stability limit can be achieved by combining the state feedback with the turbine fast valving.

Thus the state feedback used for decoupling is having an over-all beneficial effect on the system performance, both under dynamic and transient conditions over a reasonably wide operating range.

References

1 B.S. Morgan, IEEE Trans. Autom. Contr., 9 (1964) 405.
2 P.L. Falb and W.A. Wolovich, IEEE Trans. Autom. Contr., 12 (1967) 651.
3 P.J. Nolan, N.K. Sinka and R.T.H. Alden, Int. Jrl. Control, 19 (1974) 1177.
4 K. Raja Reddy and M.P. Dave, IEEE PES Summer Meeting, paper No. A75, 1975, p. 441.
5 D.G. Luenberger, IEEE Trans. Autom. Contr., 14 (1969) 380.
6 E.J. Dabison and N.S. Rau, IEEE Trans. Power App. & Syst., 90 (1971) 2123.
7 B. Habibullah and Yao-Nan Yu, IEEE Trans. Power App. & Syst., 93 (1974) 1498.
8 W.A. Morgan et al., IEEE Trans. Power App. & Syst., 90 (1971) 1.
9 R.W. Cushing et al., IEEE Trans. Power App. & Syst., 90 (1971) 2517.
10 P.L. Dandeno et al., IEEE Trans. Power App & Syst., 87 (1968) 190.
11 M.A. Laughton, Proc. Inst. Elec. Eng., 113 (1966) 325.
12 L.M. Silverman, IEEE Trans. Autom. Contr., 15 (1970) 487.
13 IEEE Committee Report, IEEE Trans. Power App. & Syst., 92 (1973) 1904.
14 K. Prabhashankar and W. Janischewsyz, IEEE Trans. Power App. & Syst., 87 (1968) 73.

List of symbols

ϕ_d, ϕ_q = d-axis and q-axis flux linkage
i_d, i_q = d-axis and q-axis components of armature current

ϕ_{fd} = d-axis field flux linkage
v_d, v_q = d-axis and q-axis components of terminal voltage V_t
V_b = Infinite busbar voltage
v_{fd} = Equivalent field voltage
V_r = Voltage regulator reference voltage
v_s = Derivative stabilizing signal
x_d, x_q = d-axis and q-axis steady state reactances.
x'_d = d-axis transient reactance
x_e = Equivalent transmission line reactance
τ_f = Open circuit field time constant
τ_x = Exciter time constant
τ_s = Stabilizing loop time constant
τ_{ch} = Steam chest time constant
μ = Voltage regulator open loop gain
μ_s = Gain of derivative stabilizing loop
k_g = Speed governor loop gain
D = Damping constant, including effect of damper circuits
M = Inertia constant
P, Q = Active and reactive power at generator terminals
P_t = Turbine power output
P_u = Electrical output of generator
u_t = HP inlet valve actuating signal
u_r = Exciter actuating signal
HP, LP, IP = High pressure, low pressure and intermediate pressure
δ = Rotor angle
pu = Per unit
s = Laplace transform variable
pf = Power factor
P = Differential operator d/dt
FCT = Fault clearing time
Δ = Used for linearized quantity
x = State vector
y = Output vector
u = Control input vector

Appendix A

The flux linkage equations are given by

$$\begin{bmatrix} \phi_{fd} \\ \phi_d \\ \phi_q \end{bmatrix} = \begin{bmatrix} 1 & -(x_d - x'_d) & 0 \\ 1 & -x_d & 0 \\ 0 & 0 & -x_q \end{bmatrix} \begin{bmatrix} i_{fd} \\ i_d \\ i_q \end{bmatrix} \quad \text{(A1)}$$

The voltage equations are given by

$$\begin{bmatrix} v_{fd} \\ v_d \\ v_q \end{bmatrix} = \begin{bmatrix} 1 + \tau_f p & -(x_d - x'_d)\tau_f p & 0 \\ 0 & 0 & x_q \\ 1 & -x_d & 0 \end{bmatrix} \begin{bmatrix} i_{fd} \\ i_d \\ i_q \end{bmatrix} \quad \text{(A2)}$$

$$v_q = V_b \cos \delta + x_e i_d$$

$$v_d = V_b \sin 6 - x_e i_q \quad \text{(A3)}$$

$$v_t^2 = v_d^2 + v_q^2$$

Appendix B

Calculation of transformation matrix M

For small signal operation, from eqns. (A1)—(A3), we have

$$\Delta_{i_{fd}} = [(x_d - x'_d)/X'_d]\ V_b \sin \delta\ \Delta \delta + (X_d/X'_d)\ \Delta \phi_{fd}$$

$$= m_{31}\ \Delta \delta + m_{33}\ \Delta \phi_{fd}$$

The non zero elements of M are $m_{11} = m_{22} = m_{44} = m_{55} = m_{66} = 1$
$m_{31} = (x_d - x'_d)\ V_b \sin \delta / X'_d$, $m_{33} = X_d/X'_d$

where $X_d = x_d + x_e$, $X'_d = x'_d + x_e$

Appendix C

Elements of A and $\bar{C}$ matrices

$$a_{21} = \frac{1}{\bar{M}}[A_1 - A_2 m_{31}/m_{33}],\ a_{22} = -D/\bar{M},\ a_{23} = \frac{A_2}{\bar{M}}\frac{1}{m_{33}}$$

$$a_{31} = \frac{1}{\tau_f}(m_{33}A_3 - A_4 m_{31}),\ a_{32} = m_{31},\ a_{33} = A_4/\tau_f,\ a_{34} = m_{33}/\tau_f$$

$$a_{54} = -\frac{\mu_s}{\tau_s \tau_x},\ a_{55} = -\frac{1}{\tau_s} - \frac{\mu \mu_s}{\tau_x \tau_s},\ b_{51} = \frac{\mu \mu_s}{\tau_x \tau_s}$$

$$C_{11} = A_5 - A_6\ m_{31}/m_{33},\ C_{13} = A_6/m_{33},\ C_{21} = A_7 - A_8\ m_{31}/m_{33},$$

$$C_{23} = A_8/m_{33}$$

where A_1 to A, are given by

$$A_1 = \frac{V_b}{X'_d}(\phi_q + i_q x'_d) \sin \delta - \frac{V_b}{X_q}(\phi_d + i_d X_q) \cos \delta$$

$$A_2 = \frac{\phi_q - i_q x_e}{}, \quad A_4 = -\frac{X_d}{X'_d}$$

$$A_3 = \frac{-V_b}{X'_d}(x, -x'_d) \sin \delta$$

$$A_5 = \frac{V_b \sin \delta}{X'_d}(v_q - i_d x'_d) - \frac{V_b \cos \delta}{X_q}(v_d + i_q X_q)$$

$$A_6 = \frac{v_q + i_d x_e}{X'_d}, \quad A_8 = \frac{v_d + i_q x_e}{X'_d},$$

$$A_7 = \frac{V_b \cos 6}{X_q}(v_q + i_d x_q) \frac{V_b \sin 6}{+ X'_d}(v_d - i_q x'_d)$$

where $X_q = x_q + x_e$

Journal of Applied Science and Engineering A, 2 (1977) 91—100

A SIMPLE METHOD OF DETERMINING THE AMPACITY OF EHV-OVERHEAD LINES

M.J. VOETEN

N.V. KEMA, Arnhem (The Netherlands)

(Received June 8, 1976)

Summary

The current-carrying capacity (ampacity) of overhead lines is first and foremost a thermal problem. This question has been dealt with in several articles, but, as far as is known, there is no method which provides a simple solution. In the present article, however, a method is given by which one can easily find the ampacity under varying weather conditions such as wind velocity and ambient temperature.

1. Introduction

The calculation of the ampacity of overhead lines is in fact a purely thermal problem, the production of heat being caused by the presence of an electrical current and sunshine, whereas the removal of heat occurs by convection and by radiation. As soon as the removal of heat equals the production, a condition of equilibrium exists with a constant conductor temperature. Then the following formula applies:

$$I^2 R_{\sim} + W_z = W_c + W_r$$

where

I = admissible current
$R_{\sim}$ = AC-resistance at the attained temperature
W_z = heat absorbed from sunshine
W_c = heat removed by convection
W_r = heat removed by radiation

Beginning with a particular final conductor temperature it is possible to

determine at different weather conditions the values of the components W_z, W_c and W_r for the conductor considered. After that the Joule losses can be determined and thus the admissible current. In the following the different components will be discussed separately.

2. Solar heat

The amount of heat received by a flat surface normal to the sun's rays depends very much on the clearness of the atmosphere, the solar altitude and the nature of the surface. From measurements [1] it is known that the maximum heat received by a black surface at sea level ($H_c = 90°$) can be about 1040 W m^{-2}. The solar heat absorbed by a conductor can be calculated using the formula

$$W_z = \alpha d W_n \sin \delta \qquad (\text{W m}^{-1})$$

where

a = solar absorption coefficient of the conductor
d = conductor outside diameter (m)
W_n = solar heat absorbed by a standard surface normal to the sun's rays (W m^{-2})
δ = arc cos{cos $H_c \times$ cos $(Z_c - Z_l)$}

where

H_c = solar altitude
Z_c = azimuth of the sun
Z_l = azimuth of the conductor

Starting from the most unfavourable situation ($Z_c - Z_l = 90°$) one can show $\delta = 90°$. Hence the formula for W_z becomes

$$W_z = \alpha d W_n$$

W_n depends on H_c and varies at sea level and at altitude 52° north from 575

TABLE 1

Maximum solar heat per month

Month	W_n (W m^{-2})
January, December	700
February, November	800
March, October	900
April, September	950
May, August	980
June, July	1000

W m^{-2} (December 21st) to 1005 W m^{-2} (June 21st). These values are valid for the Netherlands in its entirety.

The value of W_n to be used in any specified month is given in Table 1.

3. Convection

From the literature [2,3] it is known that the convected heat loss can he calculated by the formulas

$$W_{c1} = \left\{1.01 + 1.35 \frac{V_\perp d^{0.52}}{\upsilon_f}\right\} k_f \theta \qquad (\text{W m}^{-1})$$

and

$$W_{c2} = 0.75 \frac{V_\perp d^{0.60}}{\upsilon_f} k_f \theta \qquad (\text{W m}^{-1}),$$

respectively

where

$V_\perp$ = wind velocity normal to line (m s^{-1})
d = conductor diameter (m)
υ_f = kinematic viscosity of air ($m^2 s^{-1}$)
k_f = thermal conductivity of air (W m^{-1} °C^{-1})
θ = mean temperature rise of conductor surface (°C)

The formula W_{c1} has to be used for $0.1 < Re < 1000$, and the formula W_{c2} is valid for $1000 < Re < 50000$, where $Re = V_\perp d/\upsilon_f$ = Reynolds' number. In almost all cases Re exceeds 1000, so that as a rule the formula W_{c2} can be used.

The coefficients k_f and υ_f are dependent on temperature; they are given as a function of the average temperature T_f of the air film which forms the change-over between the conductor with temperature T_c and the surrounding air with temperature T_a; therefore $T_f = 0.5$ (T, + T_c).

The formulas given for W_{c1} and W_{c2} are not valid for $V_\perp = 0$; in this case the following expression can be used [3,4]:

$$W_{c0} = (3.71, ..., 4.14)\, d^{0.75} \theta^{1.25} \qquad (\text{W m}^{-1})$$

In the following the coefficient 4 has been used:

$$W_{c0} = 4\, d^{0.75} \theta^{1.25} \qquad (\text{W m}^{-1})$$

It is possible to introduce a drastic simplification of the above formulas (only valid for the conditions in the Netherlands), without losing the accuracy of the calculation.

To realize this the following restrictions have been introduced

$0.010 \leq d \leq 0.025$ m for copper conductors

$0.015 \leq d \leq 0.040$ m for ACSR

These restrictions, however, apply to practically all the conductors which are used in practice. The maximum temperature allowed for the conductors is in

agreement with the practice abroad, namely 70"C for copper conductors and 80"C for ACSR.

The results of the simplification are given in Table 2. Except for $V_\perp = 0$ the formulas obtained are linear. The constants k and p depend on $V_\perp$.

Investigations [5,6] have made it clear that varying the angle of attack of the wind makes a difference for the local heat transfer. Fig. 1 shows that in the most unfavourable case (angle of attack = 0°) the heat loss is hardly more than 40% of the value in the most favourable case (angle of attack = 90°). The values mentioned have been found using a thin taut wire; in practice the sag of the conductor will have a favourable influence. In the cases with $V_\perp \geq 1$ m s^{-1} it can be stated that W_{c90} is proportional to $V_\perp^{0.6}$. On that basis it can be computed that if $V_\perp$ is halved (original value $\geq$ 2 m s^{-1}), W_{c90} will be 34% lower. If $V_\perp$ is reduced to 1/3 of its original value ($\geq$ 3 m s^{-1}), W_{c90} will he 48% lower.

On the basis of Fig. 1 it can be established which reduction of $V_\perp$ has the same effect as the fact that the prevailing wind is not normal to the direction of the overhead line ($\beta \neq 90$") (see Table 3).

This shows that for a general and simple application of the determination of the ampacity as indicated in this article, allowance has to be made for a very small value of β, if not $\beta = 0$.

In view of the fact that the direction of the wind is not constant, it may be advisable to use $\beta = 9°$. When this is done, it is safe to use in the formula for W_c an "effective" wind velocity which is one third of the real wind velocity.

Moreover it is important to know the minimum wind velocity for the computation of the ampacity. Corresponding to the American and German standards, the value of 0.6 m s^{-1} normal to the conductor has been chosen with the restriction that this may only be used when the temperature of the air is relatively high.

TABLE 2

Simplified formulas for W_c

$V_\perp$ (m s^{-1})	Copper; $T_c = 70°$ C; 0 010 $\leq d \leq$ 0 025 m		ACSR, $T_c = 80°$ C; 0.015 $\leq d \sim$ 0.040 m	
	W_c (W m^{-1})	k	W_c (W m^{-1})	p
0	$(8.3\,d + 0.046) \times \theta^{1.25}$		$(7.5\,d + 0.062) \times \theta^{1.25}$	
0.6	$(32.0\,d + 0.50) \times \theta$		$(24.0\,d + 0.64) \times \theta$	
1	$(37.3\,d + 0.71) \times \theta$		$(38.6\,d + 0.63) \times \theta \times p$	1.00
2	$(69.8\,d + 0.75) \times \theta \times k$	1.00	$(38.6\,d + 0.63) \times \theta \times p$	1.52
3	$(69.8\,d + 0.75) \times \theta \times k$	1.28	$(38.6\,d + 0.63) \times \theta \times p$	1.93
4	$(69.8\,d + 0.75) \times \theta \times k$	1.52	$(38.6\,d + 0.63) \times \theta \times p$	2.30
5	$(69.8\,d + 0.75) \times \theta \times k$	1.73	$(38.6\,d + 0.63) \times \theta \times p$	2.63
6	$(69.8\,d + 0.75) \times \theta \times k$	1.93	$(38.6\,d + 0.63) \times \theta \times p$	2.93
7	$(69.8\,d + 0.75) \times \theta \times k$	2.12	$(38.6\,d + 0.63) \times \theta \times p$	3.21

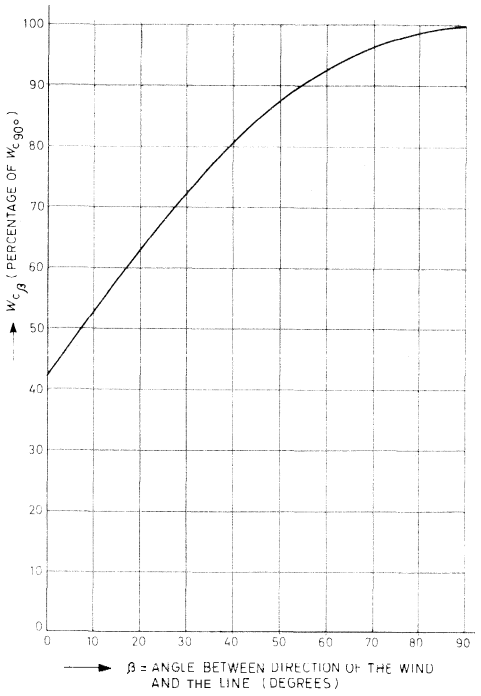

Fig. 1. Influence of the direction of the wind

Relatively high temperatures generally appear with the arrival of hot air, so with any wind. This is illustrated in Table 4, where a summary of maximum temperatures per month is given for the period 1965 to 1970. The wind velocity is also included. This information has been gathered from the day reports of the KNMI (Royal Dutch Meteorological Institute) covering 31 measuring points in the Netherlands. The average value of the measured wind velocities is 4 m s^{-1}.

The fact that at relatively high temperatures it may be assumed that $V_\perp \geqq 0.6$ m s^{-1} does not rule out the necessity of taking a value of $V_\perp \leq 0.6$

TABLE 3

Influence of the direction of the wind

β (°)	W_c/W_{c90}	f *
9	0.52	1/3
23	0.66	1/2
36	0.78	2/3

* f is the coefficient required with which to multiply V in order to get a "fictive" value of $V_\perp$. Naturally this "fictive" value is not the same as the component of V normal to the conductor.

TABLE 4

Wind velocity at high ambient temperatures

Month	T_{max}	V	Date	Measuring point(s)
January	14	3 4	29-1-'67	Woensdrecht, Hoek van Holland
February	14	7 10	22-2-'66	Twente, Eindhovcn,
March	25	5	29-3-'68	Soesterberg
April	29	3.5 5	21-4-'68	Twente, Soesterberg *
May	30	3.5 5	13-5-'69	Volkel, Eindhoven *
June	30	1 ..... 4.5	10-6-'66	Twente, IJmuiden *
July	34	4 ..... 5.5	2-7-'68	Woensdrecht, Zd. Limburg
August	31	2.5 4	13-8-'66	Woensdrecht, Zd. Limburg *
		0.5	1-8-'67	Ypenburg
		2.5 5	2-8-'69	De Bilt, Zd. Limburg *
September	28	3	26-9-'67	Eindhoven
		4 ..... 5.5	12-9-'69	Deelen, IJmuiden
October	23	2	6-10-'69	Zd. Limburg
		1 ..... 3.5	9-10-'69	Soesterberg, Deelen *
November	18	1 ..... 3.5	7-11-'65	Volkel, Eindhovcn *
		2	6-11-'66	Twrntc
		1.5 ..... 2.5	1-11-'68	Zd. Limburg, Twente
December	13	15	5-12-'65	Socstcrbcrg

* The same T_{max} at one or more other points

m s^{-1} in relevant situations. Though in general there will always be some vertical movement of the air even if there is no horizontal movement, the condition $V_{\perp} = 0$ has not been neglected in this article.

4. Radiation

There exist formulas (with slight variations) for calculating the radiated heat loss. The essential difference between these formulas can be reduced to a difference in interpretation of the heat radiated to the outside atmosphere.

In this article the formula of Webs [7] has been chosen:

$$W_r = \sigma \epsilon \pi d\{0.75 (T_c^4 - T_a^4) + 0.25 (T_c^4 - T_s^4)\} \qquad (W\ m^{-1})$$

where

σ = Stefan-Boltzmann constant = 5.68 X 10^{-8} ($W\ m^{-2}\ °K^{-4}$)
ϵ = total emissivity of conductor surface
T_c = end temperature of conductor (°K)
T_a = ambient temperature (°K)
T_s = temperature of the outside atmosphere (°K)
d = conductor outside diameter (m)

The above formula makes allowance for a part of W_r which can be radiated to the outside atmosphere (clear weather). This supposition is allowed

TABLE 6

"Maximum" ambient temperature per month

Month	"Maximum" ambient temperature T_a "max" (C and K resp)	
January, February, December	10	283
March, November	15	288
April, October	20	293
May, September	25	298
June, July, August	30	303

because W_z has also been calculated for clear weather, whilst both components eliminate each other almost entirely.

For the "maximum" air temperature per month in the Netherlands, see Table 5. This table has been derived from a publication of the KNMI [8], and covers a period of 30 years. The "maximum" temperature means the temperature that will generally be the maximum temperature in the month indicated. If the temperature rises just slightly above the given value, it will have only very little influence on the ampacity.

After substituting $T_s = 217°$ K [9] it follows that:

$$W_r = 17.84\, \epsilon d \left\{ \left(\frac{T_c}{100}\right)^4 - 0.75 \left(\frac{T_a}{100}\right)^4 - 5.54 \right\} \qquad (\mathrm{W\ m^{-1}})$$

This formula has also been very much simplified with due observance of the required accuracy.

$$\left.\begin{aligned} W_r &= (12\theta + 940)\, \epsilon d \ \text{(ACSR)} \\ W_r &= (12\theta + 760)\, \epsilon d \ \text{(copper)} \end{aligned}\right\} \quad (\mathrm{W\ m^{-1}})$$

Restrictions: $T_c = 343°$ K (copper) and 353° K (ACSR), respectively.

5. Ampacity

All the parts of the heat balance have now been discussed. It is now possible to compute the ampacity of a certain conductor in a short way. It also is possible to use an even shorter way, because some simplified formulas have been developed for W_t as a function of $V_\perp$, in which $W_t = W_c + W_r - W_z$. For these simplified formulas see Table 6.

To obtain these formulas it was necessary to eliminate the coefficients a and ϵ. Therefore the supposition is made that the conductor has been exposed to the influence of the surroundings (oxidation and pollution). For this condition one may use $a = \epsilon = 0.6$ as is done abroad [7,10].

It turned out not to be possible to use only one formula when $V_\perp = 0$. A better result can be obtained by using two formulas, viz. one for

TABLE 6

Simplified formulas for W_t (W m^{-1} °C^{-1})

$V_\perp$ (m s^{-1})	Copper. T_c = 70° C; $\alpha = \epsilon = 0.6$; $40 \leqslant \theta \leqslant 90$°C; $0.010 \leqslant d \leqslant 0.025$ m	ACSR T_c = 80 C; $\alpha = \epsilon = 0.6$, $50 \leqslant \theta \leqslant 100$°C; $0.015 \leqslant$ d $\leqslant 0.040$ m
0	26.9 d + 0.12 *	27.7 d + 0.18 *
0.6	35.6 d + 0.50	30.5 d + 0.64
1	40.9 d + 0.71	45.1 d + 0.63
2	73.4 d + 0.75	65.2 d + 0.96
3	92.9 d + 0.96	81.0 d + 1.22
4	109.7 d + 1.14	95.3 d + 1.45
5	124.4 d + 1.30	108.0 d + 1.66
6	138.3 d + 1.45	119.6 d + 1.85
7	151.6 d + 1.59	130.4 d + 2.02

* Formula valid for $T_a > 5$°C. For $T_a \leqslant 5$°C use 31.8 d + 0.14 (copper); 31.2 d + 0.19 (ACSR). (For practical use T_a and T_c are expressed in °C instead of °K).

-20°C $\leq T_a \leq 5$°C and one for 5"C $< T_a \leq$ **30°C.**

To compute the heat $W_t = I^2R_\sim$ produced by a certain current it is necessary to know the AC-resistance at the temperature the conductor has reached. It is rather simple to compute this resistance for copper conductors, because only the skin effect will have to be taken into account. This skin coefficient [11] is given in Fig. 2 with t/d = 0.

For ACSR it is necessary not only to make allowance for the skin effect, but also for the eddy current and hysteresis losses in the steel core of the conductor. The aluminium wires wound around the core in one or more layers form a solenoid per layer. Because the current almost entirely flows through the length of the wires and only for a very small part from wire to wire, this current will have a strong magnetic effect, causing eddy current and hysteresis losses. These losses will increase the AC-resistance.

Investigations [12,13] have found that there is a clear difference between conductors with an odd and with an even number of aluminium layers. The explanation for this is that the different layers are in general wound in opposite directions, so that per two layers the magnetic effect can be neglected. This is the reason why it can be stated that for conductors having an even number of aluminium layers the only effect to be considered is the skin effect.

On the other hand the magnetic effect of conductors having only one layer of aluminium will be high. However, it is very difficult to compute this effect since it is dependent on the current and on whether the steel is saturated or not.

The manufacturer has to state the AC-resistance as a function of the current [14]. For the rest it does not seem probable that this kind of conductor will ever be used as a phase-conductor in the Netherlands. That is the reason why this problem has not been discussed in more detail.

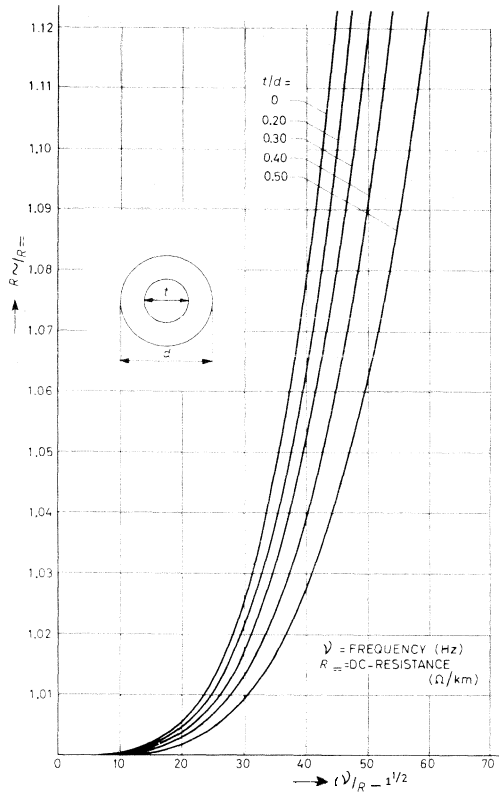

Fig. 2. Skin effect curves for round tubular conductors.

The AC-resistance of ACSR with three layers of aluminium is also dependent on the current but to a much lesser extent than for conductors with one layer. The value of the AC-resistance of a number of common ACSR-conductors with two and three layers, respectively, is given in Table 7.

The accuracy of the simplified formulas for W_t has been tested with the conventional formulas. It turned out that the current calculated with the simplified formulas for W_t (and $W_t = I^2 R_\sim$) is never more than 1% higher and never more than 3% lower than the current calculated with the conventional formulas. This accuracy for W_t mentioned above does not include the situation where $V_\perp \approx 0$. The values for the current under this condition may be at most 5% higher or lower than those calculated with the conventional formula.

It is now important to define the expression "nominal current". It is proposed to define the "nominal current" as the current that under the conditions $T_a = 30°C$, $V_\perp = 0.6$ m s^{-1}, $\alpha = \epsilon = 0.6$ and maximum solar heat leads to the end-temperature of the conductor, being 70°C for copper and 80"C for ACSR. In this manner the nominal current has been computed for a number of conductors used in the Netherlands (see Table 8).

TABLE 7

AC-Resistance

ACSR	Type	Diam. ($\times 10^{-3}$ m)	Number of layers of aluminium	$R_{=80}$ (Ω/km)	$R_{\sim}/R_{=}$	$R_{\sim 80}$ (Ω/km)
25/152	Ostrich	17.28	2	0.236	1.01	0.238
321185	Ibis	19.20	2	0.196	1.01	0.198
20/224	PNEM	20.34	3	0.159	1.03	0.164
401240	DIN	21.70	2	0.153	1.01	0.155
23/259	Groningen	21.84	3	0.138	1.03	0.142
531322	Grosbeak	25.15	2	0.111	1.01	0.112
371424	SEP	27.94	3	0.085	1.04	0.088
391457	PGEM	29.98	3	0.079	1.04	0.082
63/483	Cardinal	30.38	3	0.074	1.04	0.077
52/591	EZH 1,3	33.02	3	0.060	1.04	0.062
771604	Crackle	33.99	3	0.060	1.04	0.062
60/686	EZH 1,4	35.56	3	0.063	1.05	0.056

Although it does not seem to be necessary to make an allowance for the situation $V_{\perp} = 0$ (as one has to of course for $V_{\perp} < 0.6$ m s^{-1}), the percentage of ampacity reduction for $V_{\perp} = 0$ is given in Fig. **3.** The highest ambient temperature used for this calculation is $T_a = 25$°C. Moreover, the conductor temperature can be computed when the conductor is loaded with the

TABLE 8

Nominal current

Tvpe of conductor		I_{nom} (A)
Copper	70	330
	95	405
	120	465
	150	540
	185	615
	300	845
ACSR	251152	495
	32/185	555
	20/224	620
	40/240	650
	23/259	680
	53/322	790
	37/424	920
	391457	965
	63/483	1010
	521591	1150
	771604	1160
	601686	1240

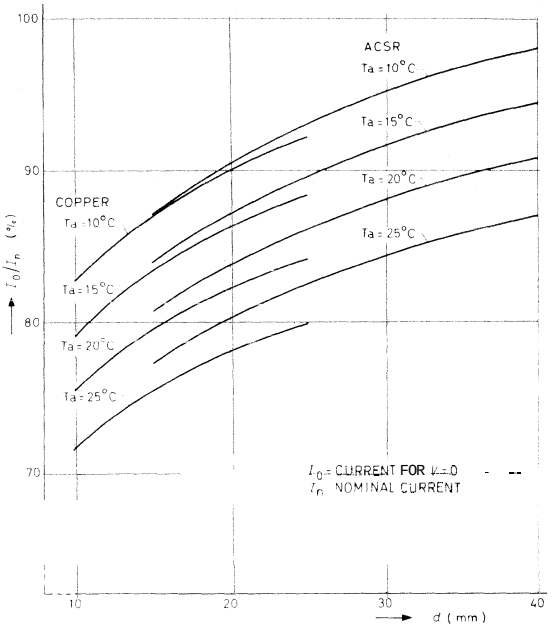

Fig. 3. Reduction of the ampacity for V = 0.

nominal current under the condition of no movement of the air at all. In this very unfavourable situation the ACSR conductor 37/424 could reach a temperature of 100°C. This very unfavourable situation only occurs when there is a coincidence of bad conditions, such as absolute calm, high ambient temperature, maximum solar heat and maximum current. So it will generally be satisfactory to carry out the computation with $V_\perp = 0.6$ m s^{-1}, though one has to remain prepared for the situation described.

Rating the arnpacity is also possible with the nomograms in Figs. 4 and 5 (copper and ACSR resp.). Fig. 4 is simpler in design, since the value of $R_\sim$ could be combined with the diameter d.

This is not (exactly) possible for ACSR-conductors. In Figs. 4 and 5 wind velocities are given up to and including 7 m s^{-1} normal to the conductor. The current calculated for $V_\perp = 7$ m s^{-1} is about twice the current with $V_\perp = 0.6$ m s^{-1}. For practical reasons it will not be suitable to have a current higher than two times the nominal one.

An example (Fig. 4) is the determination of the arnpacity for a 150 mm^2 copper conductor with $T_a = 30°$ C, $T_c = 70°$ C, $V_\perp = 0.6$ m s^{-1} and $\alpha = \epsilon = 0.6$. It can be shown that **I** = 545 A. The simplified formulas give **I** = 540 A, while the conventional method leads to **I** = 538 A.

For the ACSR conductor 37/424 one can see in Fig. 5, based on T_a = 10" C, T_c = 80"C, $V_\perp = 3$ m s^{-1} and $\alpha = \epsilon = 0.6$, that **I** is about 1670 A. The simplified method leads to **I** = 1664 A, and the conventional calculation

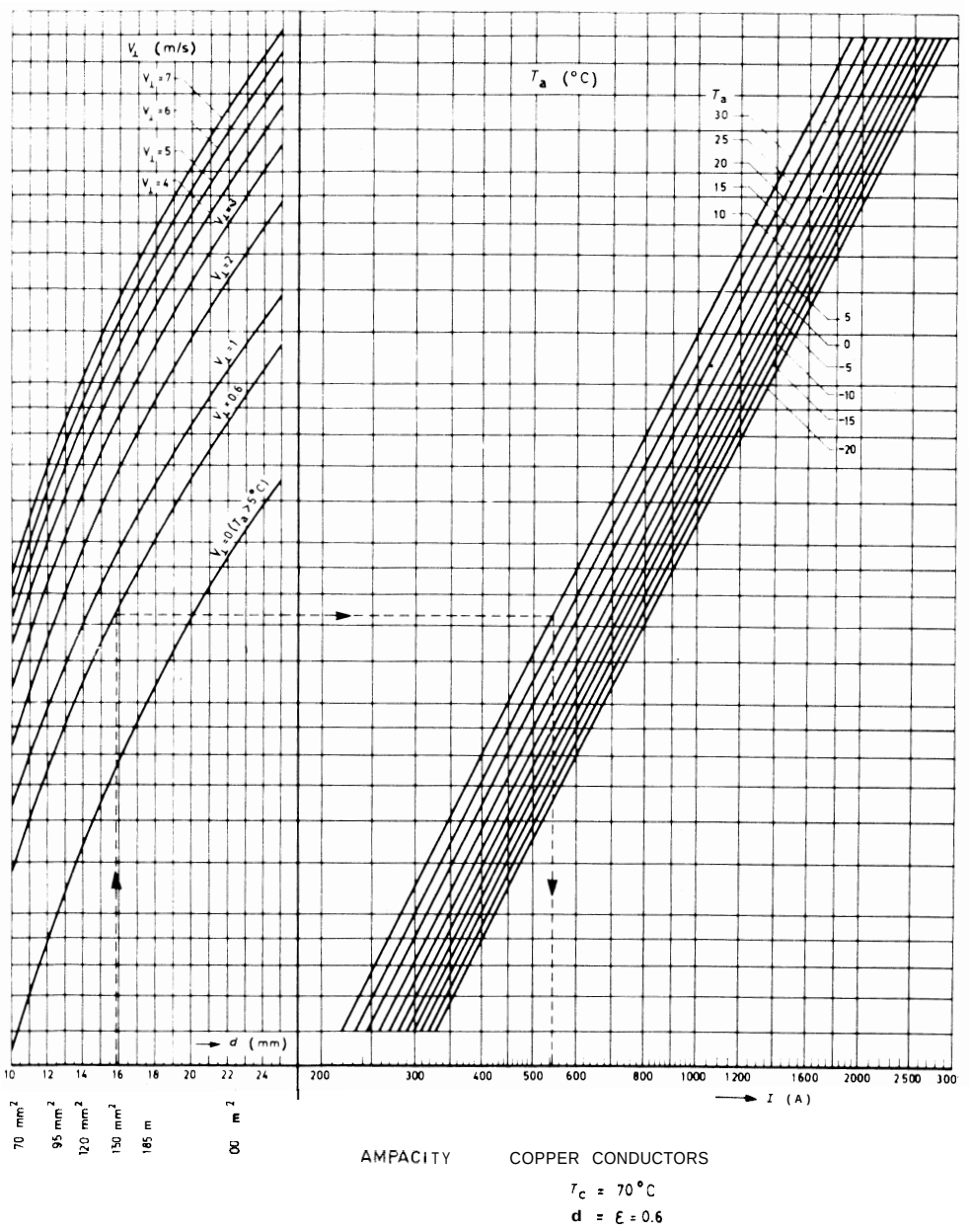

Fig. 4. Ampacity for copper conductors.

gives the result **I** = 1674 A. In both cases the deviations are very small.

As to the influence on the final result of the coefficients a and ϵ, which can be considered equal [7], it can be mentioned that for a new (not oxidized) 150 mm^2 copper conductor (all other conditions remaining the

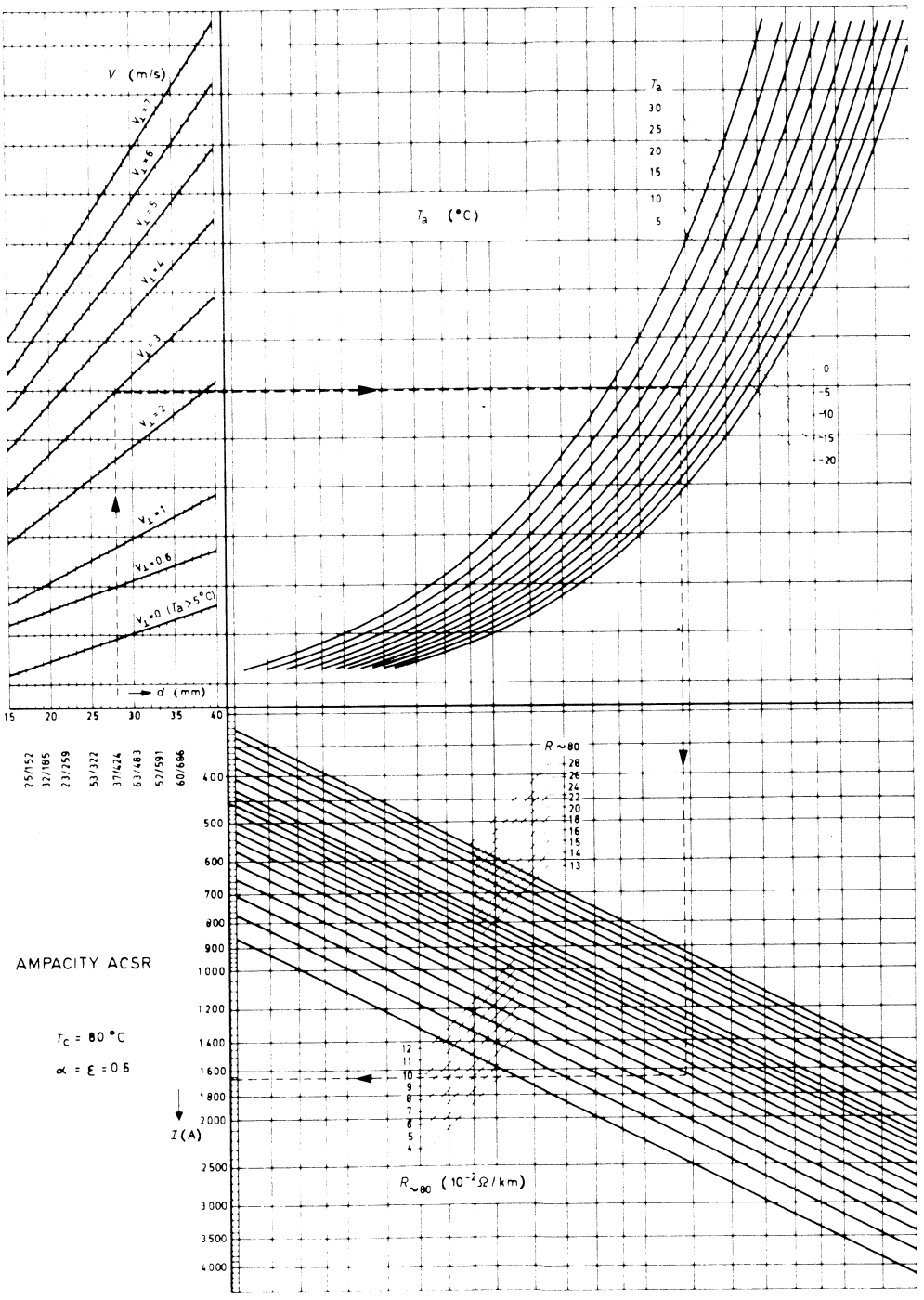

Fig. 5. Ampacity for ACSR conductors.

same as before), the simplified method would lead to **I** = 531 A. For the ACSR-conductor 37/424 one can show that **I** = 1643 A. The calculation is based on $a = \epsilon = 0.2$. It appears that in both cases tho arnpacity is about 1.5% smaller than in the case where $a = \epsilon = 0.6$. It can be proved that under the most unfavourable circumstances (large d and large θ), the arnpacity of new copper conductors is decreased by about 4.5%, whilst for ACSR-conductors the reduction is about 6%.

As for badly oxidized and contaminated conductors one should use [7] $\alpha = \epsilon = 0.9$. The present article does not enter into this problem in any more detail.

Finally, for practical purposes, Table 9 gives a survey of the admissible current during the month, based on $V_\perp = 0.6$ m s^{-1} and $a = \epsilon = 0.6$. The different "maximum" temperatures mentioned in Table 5 are also considered.

From Table 9 it can be calculated that the "winter rating" of copper conductors is about 22% higher than the "summer rating". For ACSR conductors the difference is about 18%.Naturally, the different values for T_c with respect to copper- and ACSR conductors respectively show this seasonal dependence.

TABLE 9

Allowable current for $V_\perp = 0.6$ m s^{-1}, $a = \epsilon = 0.6$

		June, July, August,	May, September,	April, October,	March, November,	February, January, December
T "max." (°C)		30	25	20	15	10
Copper	70	330	350	365	385	400
	95	405	430	455	475	495
	120	465	495	520	545	570
	150	540	570	600	630	660
	185	615	655	690	725	755
	300	845	895	945	990	1035
ACSR	25/152	495	520	540	565	585
	32/185	555	585	610	635	660
	201224	620	650	680	705	735
	40/240	650	680	710	740	765
	23/259	680	710	740	770	800
	53/322	790	830	870	905	935
	371424	920	965	1010	1050	1090
	39/457	965	1010	1055	1100	1140
	631483	1010	1060	1105	1150	1195
	52/591	1150	1210	1260	1315	1365
	77/604	1160	1220	1275	1325	1375
	601686	1240	1300	1360	1415	1470

6. Conclusion

By means of the simplified method of calculation dealt with in this paper, it is possible to determine quickly the ampacity of EHV-overhead iines. By doing so this ampacity can be adjusted directly for the prevailing conditions such as wind velocity and ambient temperature. Although, strictly speaking, this calculation applies only to singular conductors, it may also be used for bundle conductors since, in general, the mutual thermal influence of the sub-conductors can practically be neglected.

Keferences

1 Heating, ventilating and airconditioning guide, American Society of Heating and Ventilating Engineers, New York, 1956.
2 W. McAdams, Heat transmission, McGraw-Hill, New York, 3rd ed., 1954.
3 H. House and P. Tuttle, Current-carrying capacity of ACSR, IEEE Trans. Power App. & Syst,., 78 (1959) 1169.
4 H. Seelye and A. Malmstrom, Current ratings of overhead conductors, Electr. Light & Power, (1943).
5 V. Morgan, Rating of bare overhead conductors for continuous currents, Proc. Inst. Elec. Eng., 114 (1967) 1473.
6 K. Ewelt, H. Kollewe and U. Stoll, A thermal model for determination of temporary overhead line ampacity dependent on weather conditions, Cigre, Rept. 22-04, 1970.
7 A. Wells, Dauerstrombelastbarkeit von Freileitingsseilen aus Kupfer, Aluminium und Aldrey, Elektrizitatswirtschaft, (1963) 23.
8 KNMI — Frequency tables according to the measurements at De Bilt in the Period 1931 — 1960, KNMI, De Bilt, 1970.
9 Hütte, I., Theoretische Grundlagen, Akademischer Verein Hutte, Berlin, 1955.
10 J. Gorub and E. Wolf, Load capability of hare ACSR and all-aluminium conductors, IEEE Trans. Power App. & Syst., 82 (1963) 852.
11 W. Lewis and P. Tuttle, Resistance and reactance of' ACSR, IEEE Trans. Power App. & Syst., 77 (1959) 1189.
12 L. Matsch and W. Lewis, Magnetic properties of ACSR core wire, IEEE Trans. Power App. & Syst., 77 (1959) 1178.
13 V. Morgan, Electrical characteristics of steelcored aluminium conductors, Proc. Inst. Elec. Eng., 112 (1965) 325.
14 ALCOA — Resistance and reactance of aluminium conductors, Section 5, Aluminium Corporation of America, Pittsburg, 1960.

Journal of Applied Science and Engineering A, 2 (1977) 107—116

A MATHEMATICAL MODEL FOR SIMULATING THE HYSTERETIC BEHAVIOUR OF MAGNETIC MATERIALS

J.H.J. FLUITMAN and F.W. UILHOORN *

Department of Electrical Engineering, Twente University of Technology, Enschede (The Netherlands)

(Received May 19, 1976; in revised form June 30, 1976)

Summary

A mathematical model is proposed by which an experimentally determined dependence of magnetization on magnetic field can be approximated. The model includes a description of major and minor loops, of any order, and can he used to compute the magnetic behaviour for any sequence of magnetic field values. The description can be classified as a model based on the use of a relatively small number of parameters and can be applied to serve a variety of purposes.

1. Introduction

Simulation by means of a digital computer of the behaviour of systems containing magnetic materials with hysteresis requires a programmable model of the hysteretic characteristics. A variety of models have been developed and published so far, which satisfy a diversity of requirements depending on the character of the problem and the desired accuracy.

The character of the problem will be determined by the field of research and by the specific questions to be answered. For example, one may be interested in the dynamic behaviour of electronic circuits containing magnetic elements, in the quasi-static behaviour of electromechanical devices, or referring to our own work at the Twente University, in the write and read process in digital magnetic recording.

* Now with National Aerospace Laboratory, Amsterdam, The Netherlands.

With respect to accuracy, it goes without saying that the more accurate a model is, the greater will be its complexity. So accuracy means an increasing number of parameters (and time of computing) and a loss of transparency of the model, and requires increasing efforts in fitting the model to actual hysteresis loops. On the other hand, in a less accurate model errors will accumulate, to a large extent, when derived values are used as starting points in successive steps. The choice of a model will be a compromise between accuracy and simplicity and will be dictated, in the end, by the purpose of the user and the computing facilities that are at his disposal.

Examples of models using a large number of parameters are the one proposed by Portigal [1], which approximates the major loop by means of cubic splines, and the one proposed by Hay and Chaplin [2], which considers hysteretic behaviour as being generated by an aggregation of primitive non-interacting elements.

The proposal of Portigal is a purely mathematical one, very accurate indeed but applicable only in cases where a few loops have to be described. It is impracticable if one desires to express any possible major or minor loop, unless one restricts the spline description to the major loop and introduces an algorithm to derive minor loops from the major loop. This modification, however, results in a minor loop description much less accurate than the major loop description and thus gives the model a somewhat unbalanced character. The model of Hay and Chaplin is related to the physical notion on which the so-called Preisach model **[3]** is based. This physical notion leads to the expectation that the ability of the model to describe major and minor loops with great accuracy at the same time is greater than in Portigal's approach and will depend on the degree to which the model reflects physical reality.

Models containing a small number of parameters have the obvious advantage of being transparent and being easy to manipulate, and are useful when qualitative properties are studied. In the case of simulation of the write process in magnetic recording, use is generally made of relatively simple models (*e.g.* see [4–7]) which are not very accurate. This choice of simple models is partly due to the fact that they play a role in much bigger and time consuming computer programmes and partly perhaps to the fact that approximations in other parts of the programme do not justify the efforts of using very accurate hysteresis models. However, work is moving towards an ever increasing degree of sophistication in modelling and programming, which makes more complex hysteresis models acceptable and even essential when the attention is focused on the effect of the accuracy of the hysteresis model itself on the outcome of the simulation, as is the case in our investigation. The need was felt therefore to improve the existing models, this of course involving new parameters, but at the same time to keep the improvement within the class of simple models in the sense that a relatively small number of parameters is used, which may have a direct or an indirect physical significance.

Although our investigations are directed mainly to magnetic recording we believe that the model we propose can be used in many other applications as it is an empirical fact that in spite of the great diversity in magnetic materials and devices some general characteristics of hysteresis loops are common to many of them.

In the following sections we will deal with the intrinsic MH loop What we want is a description of the experimentally determined dependence of M on H that includes major and minor loops and takes into account the time order of the events. We first describe some characteristics of the MH-loops, then give a description of our model and some possible extensions and finally discuss some of its properties

2. **Characteristics** of MH-loops

Fig. **1** shows a characteristic MH-loop. A family of first order ascending minor loops is depicted, starting from the descending major loop, together with a family of second order minor loops which starts from an ascending first order minor loop. In characterizing the major loops we anticipate the presentation of our model and follow Maizieres and Fourquet [8] who propose a description by means of four similar hyperbolic parts characterized by four parameters: the saturation magnetization M_s, the coercive force H_c, the curvature of the hyperbolas p and a parameter R($R \geqslant 0$) characterizing the "shear" of the loop. The major loops are expressed as follows:

$$(M_s - \epsilon M)\,(H - RM - \alpha H_c) = pM \tag{1}$$

with $a = +1$ for the ascending loop
$a = -1$ for the descending loop

$\epsilon = +1$ for $M > 0$
$\epsilon = -1$ for $M < 0$

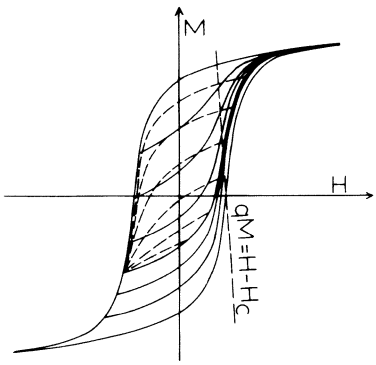

Fig. **1.** Characteristic MH-loops (magnetic tape, Philips ER 13) showing a family of first order minor loops (solid lines) and a family of second order minor loops (dashed lines). A straight line is shown, connecting the bending points in the first order minor loops.

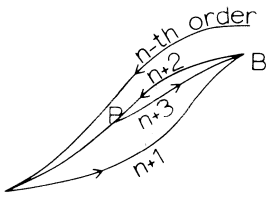

Fig. 2. A minor loop is directed between the loops of the two preceding orders to the starting point of the preceding order loop.

This model degenerates to a set of straight lines for p = 0, while for positive increasing values of p eqn. (1) represents loops with decreasing curvature.

MH-loops approach the lines $M = \pm M_s$ asymptotically. In the original model of Maizieres and Fouryuet, BH-loops and ϕi-loops can also be described. A fifth parameter is then used to characterize the inclination of the asymptotes corresponding to our lines M = $\pm M_s$. We prefer the description with four parameters to keep the formulae as simple as possible. The facility to simulate hysteresis curves which approach saturation along an inclined asymptote can be added afterwards by an appropriate roation of the loop to he simulated.

With regard to the minor loops it is important to note that any minor loop is guided more or less by the loops of preceding order. Fig. 2 illustrates what we mean by this. The (n + 2)-th order,loop is directed in the space between the two preceding ones and guided to the point A without intersection of the preceding loops. In the same way an (n + 3)-th order loop, starting at point P, is directed to B. It is important that a model reflects this property in order to prevent instability (see [9]).

A characteristic which plays an important role in the description of the minor loops in our model is the straight line which connects the bending points in the first order minor loops (Fig. 1).Of course, it is only an assumption that this line is straight at all, but Uilhoorn has noticed that this characteristic can be observed in practical cases while similar statements can be found in the literature [10,11]. We discuss this in a later section. Further details concerning MH-loop characteristics can also be found in [2].

3. Description of the model

The description of the major loops in our model is taken from Maizieres and Fourquet [8], (eqn. (1)).This model is sufficiently flexible for our purposes and more accurate than other simple models known to us (see Section 4). It is a happy coincidence that this model is suitable for a description of the minor loops in analytical form.

For this purpose we introduce the lines $qM = H - \alpha H_c$ which connect the bending points in the first order minor loops. In fact it is only the direction

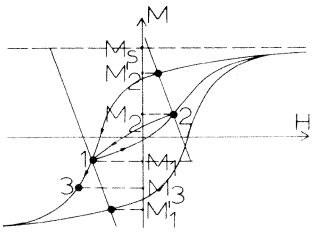

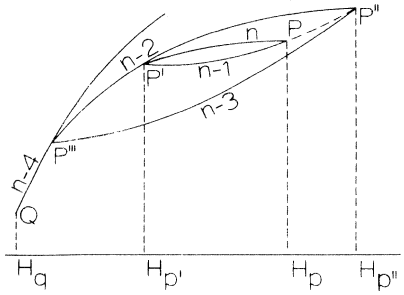

Fig 3 The first order minor loop (1→ 2) is derived from the ascending major loop by multiplication from M M_s with the factor K_1 - $(M_1$ $M_s)/(M'_1$ $M_s)$

Fig. 4. A minor loop of higher order is generated whenever a turning point (*e.g.* H_p) is situated between the last and the preceding one ($H_{p'}$ and $H_{p''}$). In other cases (*e.g.* H_q) the MH-locus returns to (a) minor loop(s) of lower order.

that we need, which is determined by the parameter q.

The model now runs as follows (see Fig. **3**): first order ascending minor loops are derived from the ascending major loop by a multiplication in the direction determined by q from a baseline M = M_s. The constant of multiplication K_1 can be calculated when the starting point on the major loop is known: $K_1 = (M_1 - M_s)/(M'_1 - M_s)$ (see Fig. *3* for the meaning of the variables). A second order descending loop is derived in an analogous way. Now the multiplication occurs from $M = M_1$ as baseline and again in the direction of q. It follows that K, $= (M_2 - M_1)/(M'_2 - M_1)$. A third order loop is derived from a first order loop in the same way, and so on. Of course the same procedure is used for a sequence of minor loops starting from the ascending major loop.

In general the n-th order loop is derived from the (n — 2)-th loop with the value of the multiplicative constant K_n determined by the coordinates of the last and the last but one turning point. The description can be completed by defining what happens when the H-value of the (n + 1)-th turning point overshoots that of the (n — 1)-th one; in that case the (n — 2)-th minor loop will be followed again. Looking at Fig. **3** this means that whenever the third turning point is situated to the left of the first one the MH-locus is on the descending major loop again. In Fig. 4 this settlement is clarified for the general case in which a field value H_p is followed by H_q. From P to P' the n-th order loop is followed, from P' to P''' the (n — 2)-th one and from P''' to Q the (n — 4)-th one.

Analytical expressions for the minor loops can be derived from the expression for the major loops, eqn. (1), to read:

$$[M_s P_n - \epsilon(M - M_n^*)]\,[\mathrm{H} - R_n(M - M_n^*) + \mathrm{Q}_n - \alpha(-1)^{n+1} H_c] = p(M - M_n^*) \quad (2)$$

with

$$\left.\begin{aligned} &P_n = P_{n-2}K_n;\ P_1 = K_1;\ P_2 = K_2 \\ &M_n^* = M_{n-1}(1 - K_n) + K_n M_{n-2}^*;\ M_1^* = \alpha M_s(1 - K_1);\ M_2^* = M_1(1 - K_2) \\ &R = \frac{R + (P_n - 1)q}{P_n} \\ &Q_n = Q_{n-2} + q(M_{n-2}^* - M_n^*);\ Q_1 = \alpha q M_s(K_1 - 1);\ Q_2 = qM_1(K_2 - 1) \end{aligned}\right\} \quad (3)$$

With the help of these recurrence relations all parameters can be calculated from the major loop parameters and the coordinates of the turning points (which also determine K_n). The proof of eqn. (2) can be given by complete induction. Transformation of eqn. (2), for n — 2, by multiplication by a factor K_n from a baseline M = M_{n-1} in the direction determined by q, gives eqn. (2) for n.

This transformation can be expressed by

$$\left.\begin{aligned} H &\to H + q(M - M_{n-1})\left(\frac{1}{K_n} - 1\right) \\ M &\to \frac{1}{K_n}(M - M_{n-1} + K_n M_{n-1}) \end{aligned}\right\} \quad (4)$$

Introducing (4) into (2) results in (2) and (3).

To compute a path in the MH-plane which corresponds with a sequence to be simulated a series of H-values of the turning points (H_1, H_2, ...etc.) must be given. If the model is programmed, a procedure has to be designed which selects the turning points from any sequence of H-values that determine the magnetic history of the material to be simulated. The value of α in eqns. (2) and (3) is determined by the starting point: $\alpha = 1$ when the starting point is on the descending major loop, $\alpha = -1$ in the other case. The value of ϵ is equal to the value of ϵ of that part of the major loop from which the minor loop part is ultimately derived. The starting situation determines the first loop. M_1 can be calculated by putting H = H_1 in eqn. (1). The resulting cubic equation (in short: $AM_1^2 + BM_1 + C = 0$) has the two roots $[-B \pm \sqrt{(B^2 - 4AC)}]/2A$. It is easy to prove that the correct solution is the root $[-B - \sqrt{(B^2 - 4AC)}]/2A$ and that this is consistently valid, regardless of the values of a, E and the order of the minor loop. (An important point in this proof is the observation that the sign of the nominator $2A = 2\epsilon R_n$ is equal to the sign of E.) Next K_1 can be calculated and the first order minor loop can be formulated. This cycle has to be repeated at any turning point: calculate M_n from H_n and the (n — 1)-th order minor loop, calculate K, from M, and so on.

The lines $qM = H - \alpha H_c$, connecting the bending points of the first order

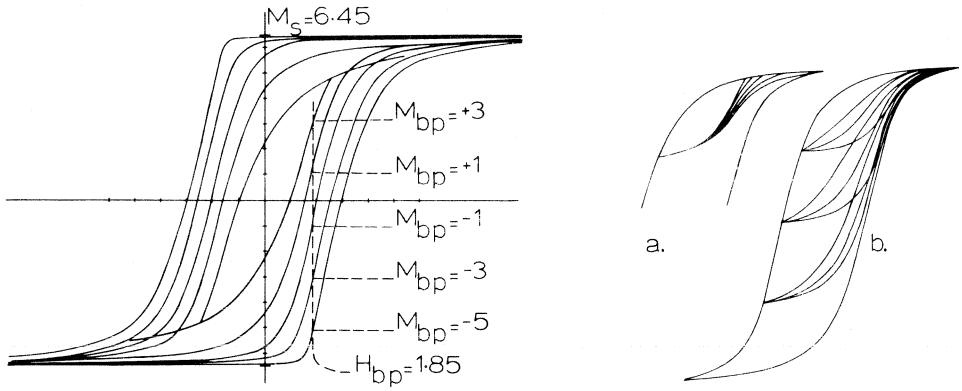

Fig. 5. Vatiation of the parameters H_{bp} and/or M_{bp} results in major loop forms of great diversity. Major loops are shown having different values of M_{bp} (—5, —3, —1, 1 and 3 resp.) with all other parameters fixed ($H_{bp} = 1.85, p = 0.2$ and $R = 0.2$). For reasons of economy thr major loops are drawn one inside the other.

Fig. 6. (a) Influence of variation of Δ (with $M_s = 6.45, H_{bp} = 1.85, M_{bp} = 1.00, P = 0.2$, q = 0.1, $R = 0.2$ and $\alpha = 1$) on a first order minor loop. Values of Δ are —0.2;—0.1: 0; 0.03 and 0.1 (loops from left to right). (b) Effect of varying the value of q (q = —0.2, 0.01 and 0.19 resp.) on first order minor loops. For this case $M_s = 6.45, H_{bp} = 1.85, M_{bp} = 1.00, R = 0.2, \alpha = 1$ and $\Delta = 0$.

loops, intersect the major loops at the points $M = 0, H = \alpha H_c$. This is simply so because of the symmetry of our model, the hyperbola parts are all similar and fit to each other at the points just mentioned, The model can be generalized, however, to represent those cases for which the bending point in the major loop no longer can be approximated by a point on the H-axis. We found it advantageous to replace the one parameter H_c by the two parameters H_{bp} and M_{bp} (see Fig. 5; bp stands for "bending point") and at the same time abandon the similarity of the hyperbola branches. This can be done without introduction of a second additional parameter. When the curvature parameter of the branches having $\alpha\epsilon = 1$ is denoted by p, we take the curvature parameter of the branches having $\alpha\epsilon = -1$ as $p' = p(M_s + M_{bp})/(M_s - M_{bp})$. In this way the branches having $\epsilon = +1$ and $\epsilon = -1$ fit to each other at the points (αH_{bp}), (αM_{bp}) with equal slope. In Fig. 5 we demonstrate the effect of this additional facility for some characteristic cases, which also results in a modified general expression for the loop of order n:

$$[M_s P_n - \epsilon(M - M_n^*)]\,[H - R_n(M - M_n^*) + Q_n - \alpha(-1)^{n+1}(H_{bp} - RM_{bp})] =$$

$$= p'(M - M_n^* - \alpha(-1)^{n+1} P_n M_{bp}) \qquad (5)$$

with

$$p' = (\tfrac{1}{2}\epsilon\alpha + \tfrac{1}{2})\,p + (\tfrac{1}{2} - \tfrac{1}{2}\epsilon\alpha)\,p(M_s + M_{bp})/(M_s - M_{bp})$$

The transformation formulae (3) remain valid for this generalization.

Another modification can be made by replacing M_s by $M_s(1 - A)$ where Δ is a correction factor. This may give better results in some cases and amounts to shifting the baseline from which the first order loops are generated. In Fig. 6a we show some results. (In addition, the effect of varying q is depicted in Fig. 6b).

There may be other special purpose modifications to improve the model for specific applications and it is our impression that these modifications can be performed easily starting from the standard programmed version of the model.

4. Discussion and conclusion

The parameter q plays an important role in the model. The introduction of this direction of multiplication leads to better results in the cases we have studied and links up with data found in the literature. Studies at the Tohoku University of Japan [10,11], on the behaviour of recording material have led to the insight that this direction may have a physical significance and that the inclination of the line is affected by particle packing density as a result of interaction fields. Their work is directed mainly on rather square hysteresis loops characteristic for oriented particulate media and for which $q < 0$. We however extend the use of q for values $q > 0$, which may appear in "leaning" hysteresis loops. Of course the physical significance of q is not clear in that case but nevertheless there is experimental evidence which justifies the use of it.

One of the advantages of our approach is the capability of the model to represent the effect of shear which may play a role in cases where applied magnetic fields are used instead of internal fields. In those cases the intrinsic MH-curve must be transformed by replacing M and H by M and H + DM (D is the shearing factor or demagnetizing factor, determined by the geometry of the device). This transformation amounts to the simple replacement of q and R by q + D and R + D in eqns. (1) and (3).

The proposed procedure for the derivation of minor loops assures stability. The model of Potter and Schmulian [7] which does not fulfill this requirement has been improved by Nishimoto et al. [9] to obtain stability. In fact our procedure is a generalization of the method of Nishimoto applied to the model of Mazieres and Fourquet.

Our impression is that the model proposed by us combines the advantages of preceding simple models while the description of any loop of any order can be given in a uniform analytic form which ultimately depends on a rather small number of starting parameters. A general statement about the accuracy is dangerous however, since the criterion for the accuracy may depend on the application. In one case the values of M are desired with great accuracy, in another case this may be required for dM/dH, for instance. Our preference for the major loop model of Mazieres and Fourquet is based on

TABLE 1

Maximum/mean error for some simple models and characteristic materials. The numbers are percentages of the saturation magnetization. (M_i is the saturation remanence, M_r/M_s is the squareness ratio)

	Ref. 7	Ref. 6	Ref. 5	Ref. 8	M_r/M_s
γFe_2O_3-tape (oriented)	23.6/9.1	13.6/4.3	10.4/3.2	6.6/3.7	*0.754*
γFe_2O_3-disc (nun-oriented)	15.4/7.7	11.0/4.9	13.6/8.4	7.7/3.4	*0.406*
Fe-film	4.4/1.9	18.2/11.1	25.3/16.2	3.4/1.6	*0.302*

the general visual impression of its accuracy which can be expressed quantitatively by calculating the magnitude of the deviation in the direction of M. In Table 1 the results of such a calculation are presented. For some simple models and some characteristic materials the mean and maximum deviations between experimental values and "best fit" model values show that, with respect to the criterion mentioned, the Mazieres and Fourquet model is generally the most accurate one.

In conclusion we mention a less agreeable feature of the model. In some cases a minor loop may intersect a preceding one in such a way as illustrated in Fig. 7. Such a situation may occur in the vicinity of the upper and lower parts of the major loop. Even the major loops will intersect each other in the generalized form of the model when $M_{bp} > 0$, this being generally for large values of H. To prevent instability in those regions a safety measure has to be inserted in the model. In our programme we have solved this problem by stating that whenever a situation as illustrated in Fig. 7 occurs the MH-locus will follow the loop of the preceding order. For Fig. 7 this means that the minor loop n + 2 is followed until S is reached, and the loop n + 1 by continuation to the right. A point of intersection can easily be detected by the value of the multiplication factor K_n. In the case of Fig. 7 the factor K_{n+3} to derive an (n + 3)-th order loop will have a value of **1** at the point S. When-

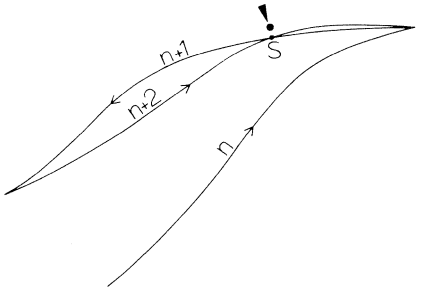

Fig. 7. Whenever a minor loop intersects a minor loop of the preceding order, the trajectory of the latter will be followed from the point of intersection onwards (to the right of point S).

ever a point is found with $K_n > 1$ this is an indication that the point is on an "overshooting" loop and must be recalculated on the loop of preceding order. It must be said that the above-mentioned feature can easily be overcome in programming and has minor influence on the applicability of the model.

Acknowledgement

It is a pleasure to acknowledge Ir. A. van Herk who initiated the work on improving hysteresis models.

References

1 D.L. Portigal, IEEE Trans. Magn., 11 (1975) 934.
2 J.L. Hay and R.I. Chaplin, Simulation, 25 (1975) 185.
3 J.G. Woodward and E. Della Torre, J. Appl. Phys., 31 (1960) 56.
4 D.L.A. Tjaden and E.J. Tercic, Philips Res. Rep., 30 (1975) 120.
5 N. Curland, An iterative hysteretic model for digital magnetic recording, Ph. D. Thesis, University of Minnesota, 1971.
6 D.J. George, S.F. King and A.E. Carr, IEEE Trans. Magn., 7 (1971) 240.
7 R.I. Potter and R.J. Schmulian, IEEE Trans. Magn., 7 (1971) 873.
8 C. Maizieres and M. Fourquet, Rev. Gen. Electr., 77 (1968) 476.
9 K. Nishimoto, M. Nagao, Y. Suganuma and H. Tanaka, IEEE Trans. Magn., 10 (1974) 769.
10 N. Tsuya and S. Sawamura, IECE Techn. Group Meeting of Magnetic Recording (in Japanese), MR 67-8 (1967).
11 S. Sawamura and S.I. Iwasaki, IEEE Trans. Magn., 6 (1970) 646.

Journal of Applied Science and Engineering A, *8* (1977) 117–121

INTEGRAL EQUA'I'IONS FOR POTENTIAL PROBLEMS WITII PERIODIC GREEN'S FUNCTIONS

G. DE MEY

Laboratory of Electronics, Ghent Slate University, Ghent (Belgium)

(Received February 5, 1976, in revised form October 26, 1976)

Summary

It is shown that a numerical integral equation method can be established to solve Laplace's equation in a geometry with a periodic structure. The method uses a periodic Green's function and requires less computation time than a conventional integral equation technique.

1. Introduction

If one has to solve Laplace's equation $\nabla^2\phi = 0$ in a geometry showing a periodic pattern in the x direction with period a, it is sufficient to solve the equation in a unit cell $0 \leqslant x \leqslant a$. in order to guarantee the periodicity of the potential, one has to fulfil the conditions that the potential ϕ and its normal derivative $\nabla\phi \,.\, \bar{u}_x$ should have the same values at x = 0 and x = a for points with the same ordinate. The problem is then reduced to an ordinary potential problem in a bounded area. This can then be solved numerically by an integral equation technique [1–3]. However, it is also possible to establish an integral equation by using a periodic Green's function with periodicity a. The potential is then automatically periodic and the boundary conditions at x = 0 and x = a may be dropped.

2. Integral equation

For the sake of simplicity, the method will be outlined for the particular geometry shown in Fig. 1. The extension to arbitrary periodic geometries with periodic boundary conditions is obvious. The shape shown in Fig. 1 is

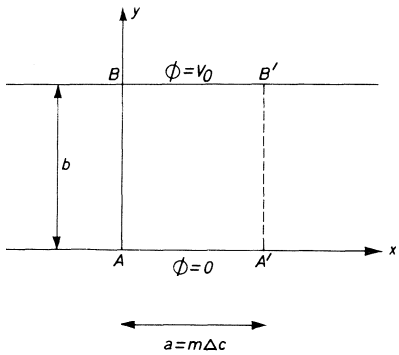

Fig. 1. Simple geometry used to establish an integral equation method with a periodic Green's function.

obviously periodic for arbitrary a values. The analytic solution is known:

$$\phi = \frac{V_0 y}{b} \tag{1}$$

so that the numerical results can easily be checked.

Jn order to determine a Green's function with a periodic character, one can proceed in the following way. The Green's function $G(\bar{r}|\bar{r}')$ being the potential in $\bar{r}$ caused by a line source in $\bar{r}'$, a periodic Green's function can easily be obtained as the potential resulting from a periodic array of line sources placed at points $\bar{r} + k\, a\, \bar{u}_x$ ($k = -\infty, \ldots +\infty$). The Green's function is then given as an infinite series which can be summed analytically. The result is [4] :

$$G(\bar{r}|\bar{r}') = \frac{1}{4\pi} \ln \left[\operatorname{ch} \frac{2\pi(y-y')}{a} - \cos \frac{2\pi(x-x')}{a} \right] \tag{2}$$

It is easily verified that (2) is periodic in the x direction.

In order to establish an integral equation the potential ϕ is written as:

$$\phi(\bar{r}) = \int_{AA'UBB'} \rho(\bar{r}')\, G(\bar{r}|\bar{r}')\, dC' \tag{3}$$

where $\rho(r')$ is an unknown function defined along AA' and BB'. If one wants to utilize the free-space Green's function p should also be defined along AB and A'B'. With the periodic function the boundary conditions on the proposed solution **(3)** yield

$$V_0 = \int_{AA'URB'} \rho(\bar{r}')\, G(\bar{r}|\bar{r}')\, dC' \text{ for } \bar{r} \in BB' \tag{4}$$

$$0 = \int_{AA'UBB'} \rho(\bar{r}')\, G(\bar{r}|\bar{r}')\, dC' \text{ for } \bar{r} \in AA' \tag{5}$$

The expressions (4) and (5) constitute an integral equation for the unknown function $\rho(\bar{r})$. Once this function has been determined, the potential ϕ can be calculated by **(3)**.

3. Numerical solution

In order to solve the integral equation numerically, the boundaries AA' and BB' are divided into m equal segments with length ΔC ($m\Delta C = a$). Denoting $\bar{r}_i$ as the centre point of the i-th interval ($i = 1, \ldots 2m$) the integral equation can be written numerically as:

$$\rho_i \int_{\Delta C_i} G(\bar{r}_i|\bar{r}')\,dC' + \sum_{\substack{j=1 \\ j\neq 1}}^{2m} \rho_j G(\bar{r}_i|\bar{r}_j)\Delta C = \begin{cases} V_0 & i = 1, \ldots, m \\ 0 & i = m+1, \ldots, 2m \end{cases} \tag{6}$$

(6) is a linear algebraic set which can easily be solved numerically in order to determine the 2m unknowns ρ_i. Once these ρ_i's are found, the potential ϕ can be evaluated by:

$$\phi(\bar{r}) = \sum_{j=1}^{2m} \rho_j G(r|r_j)\,\Delta C \tag{7}$$

For the diagonal elements of the algabraic set, an integration should be performed in order to assure convergence because $G(\bar{r}_i|\bar{r}_i) = \infty$. These diagonal elements can be calculated by:

$$\int_{\Delta C_i} G(\bar{r}_i|\bar{r}')\,dC' = -\frac{1}{2\pi}\int_0^{\Delta C/2} \ln\left(1 - \cos\frac{2\pi x'}{a}\right)dx'$$

$$= -\frac{\Delta C \ln 2}{4\pi} - \frac{1}{\pi}\int_0^{\Delta C/2} \ln\left(\sin\frac{\pi x'}{a}\right)dx' \tag{8}$$

By using the product expansion of $\sin z$ [5], one obtains:

$$\ln \sin z = \ln z + \sum_{k=1}^{\infty} \ln\left(1 - \frac{z^2}{k^2\pi^2}\right) \tag{9}$$

So that the diagonal elements are found to be:

$$\int_{\Delta C} G(\bar{r}_i|\bar{r}')\,dC' = -\frac{\Delta C \ln 2}{4\pi} - \frac{\Delta C}{2\pi}\left(\ln\frac{\pi\Delta C}{2a} - 1\right)$$

$$+ \frac{a}{\pi}\sum_{k=1}^{\infty} k\left[\frac{\Delta C}{ka} - \ln\frac{1 + \Delta C/2ka}{1 - \Delta C/2ka} - \frac{\Delta C}{2ka}\ln\left(1 - \frac{\Delta C^2}{4k^2a^2}\right)\right] \tag{10}$$

All the coefficients being known, the algabraic set can easily be solved numerically by Gauss' elimination method [6].

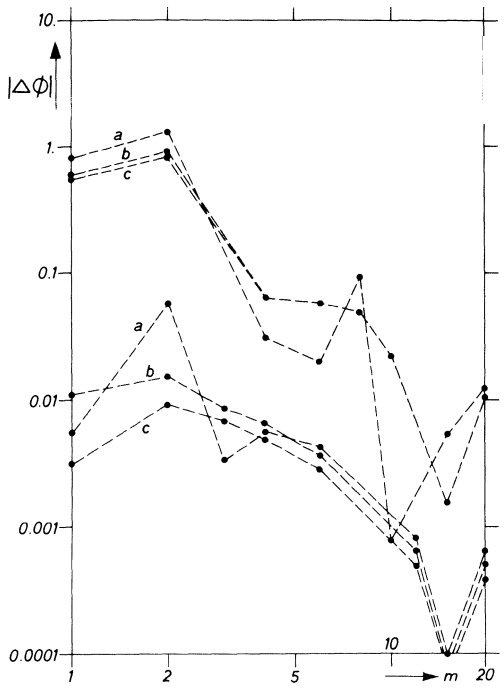

Fig. 2. Absolute value $|\Delta\phi|$ as a function of m. The upper three curves correspond to a = 4 and b = 1 and are calculated for the points x = 1.2, y = 0.2 (curvr a), y = 0.4 (curve h) and y = 0.6 (curve c). The lower three curves correspond to a = b = 1 and are calculated for the points x = 0.3, y = 0.1 (curve a), y = 0.3 (curve b) and y = 0.5 (curve c).

In Fig. 2 the absolute value of the difference between the exact values (eqn. (1), setting $V_0 = 1$, so that ϕ varies from 0 to 1), and the numerical ones are represented as a function of m for a = 1 and a = 4 (b = 1). From these results, one observes that a good accuracy can be obtained for moderate values of m. For points close to the boundary (curve a), the error shows a more irregular behaviour, which is a common feature of integral-equation methods [7,8]. It is also found that the error increases with a, which can be easily understood.

4. Conclusion

It has been proved that an integral equation method can be constructed for a geometry with a given periodicity by using a periodic Green's function. The unknown function p should then only be defined along a part of the boundary of a unit cell, which reduces the number of unknowns if the problem is solved numerically. The computation time will then also be reduced. From the numerical data obtained with a specific geometry, one

concludes that the accuracy is sufficiently high and comparable to that obtained with ordinary integral equation techniques.

References

1 T.W. Edwards and J. van Bladel, Electrostatic dipole moment of a dielectric rube, Appl. Sci. Res., 9 (1961) 151.
2 G. de Mey, Integral equation for the potential distribution in a Hall generator, Electron. Lett., 9 (1973) 264.
3 G. de Mey, A method Tor calculating eddy currents in plates of arbitrary geometry, Arch. Elektrotech., 56 (1974) 137.
4 J. van Bladel, Electromagnetic fields, McGraw Hill, New York, 1964, pp. 174—175.
5 M. Abramowitz and I. Stegun, Handbook of mathematical functions, Dover, New York, 1965, pp. 75—85.
6 T.R. McCalla, Introduction to numerical methods and FORTRAN programming, Wiley, New York. 1967, p. 171.
7 S. de Wolf and G. de Mey, Numerical methods for solving integral equations of potential problems, Inf. Process. Lett., 3 (1975) 121.
8 S. de Wolf and G. de Mey, Numerical solution of integral equations for potential problems by a variational principle, Inf. Process. Lett., 4 (1976) 136.

Journal of Applied Science and Engineering A, 2 (1977) 123—139

THE CHANNEL CAPACITY OF MULTIWIRE CABLES WITH PARALLEL CONDUCTORS

J. VAN DER PLAATS

Eindhoven University of Technology, Dept of Electr Eng, Eindhoven (The Netherlands)

(Received June 22, 1976; in revised form January 27, 1977)

Summary

The maximum channel capacity of a coaxial cable, given the power of the input signal and the power spectral density of the assumed additive white Gaussian noise, is derived.

It is then assumed that the one inner conductor of the coaxial cable is replaced by a set of n parallel conductors and that the n transmission modes, characteristic for the resulting multiwire cable, are used to form n independent communication channels. The maximum channel capacity of a transmission system built with such a multiwire cable is derived.

Computational results for n = 1, 2 and 4 show that application of a multiwire cable instead of a coaxial cable can lead to a system with a higher channel capacity or to a saving of copper for the cable conductors.

1. Introduction

Multiwire cables with twisted pairs or star quads as well as coaxial cables are well known and extensively used in analog and digital communications. The multiwire cable with twisted wires has the advantage of being well suited for space division multiplex systems. On the other hand it has the disadvantage of non-uniformity, *i.e.* the cross-section varies along the cable and therefore this type of cable is of limited importance for high-speed digital transmission. The coaxial cable has the advantage of being uniform and is therefore convenient for high-speed digital transmission. Besides, contrary to the cable with twisted wires, the coaxial cable is extraordinarily well suited for theoretical treatments, owing to the simple rotation-symmetric configuration of its cross-section.

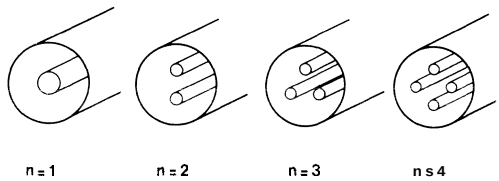

Fig. 1. Examples of n-wire cables.

It is the purpose of this paper to investigate cables that share the advantages of uniformity of the coaxial cable and of suitability for space division multiplex of the multiconductor cable. We get such a cable if we replace the inner conductor of a coaxial cable by n parallel conductors which are mutually isolated and well spaced. Some examples for different n are depicted in Fig. 1. As will be clear from this figure we will denote a cable with n parallel inner conductors surrounded by a cylindrical conducting shield as a multiwire cable with n wires, or more briefly an "n-wire cable". It is well known that such an n-wire cable can be used to form n independent transmission channels in either direction. This stems from the fact that in such a system of n + 1 parallel conductors there are in general n independent modes of propagation in either direction, corresponding to the solutions of the generalized telegraph equation [1—3]. For instance for n = 2 these modes are known as the common and the differential mode or as the even and the odd mode. Inter-channel interference between the independent transmission channels as a result of deviations from the uniformity of the cable can be coped with in the same way as with inter-symbol interference; in fact there is no principal difference between the two phenomena [4,5]. In a simple digital transmission link as well as in complicated long haul systems the transmission properties depend mainly on the combination of cable sections and the input amplifiers in the receivers that introduce gain at the appropriate points in the system. A single section, consisting of a cascade of a cable with its attenuation, phase distortion and noise and an amplifier with its amplification and its noise figure, forms a noisy channel with memory. To judge the performance of a digital communication system it can be fruitful to compare it with the performance of an ideal system. To this end we can imagine the ideal combination of an encoder and a decoder for the given noisy channel with memory and use the concept of channel capacity as introduced by Shannon [6] to judge the performance of the system. Berger and Tufts [7] call the performance of such an ideal system "the optimal performance theoretically attainable" (OPTA). The OPTA of a transmission system that follows a $\sqrt{f}$ attenuation law was given by Raisbeck [8]. The OPTA of coaxial cables was used by Pierce [9] to compare the performance of different modulation systems.

In the next part of the paper we first derive the maximum channel capac-

ity of a coaxial cable and thereupon the maximum channel capacity of an n-wire cable.

In the remainder of the paper we give some representative results of computation of these capacities and in conclusion try to evaluate these results.

2. The maximum channel capacity of a coaxial link

The performance of a coaxial cable link can be described by its channel capacity in the sense of information theory [6—9]. In this treatise we restrict ourselves to power limited channels with additive Gaussian noise. This power constraint together with the typical variation of the attenuation of the cable with frequency leads to a bandwidth constraint in the case of maximum channel capacity. The signal will contain no frequencies greater than some maximum frequency W.

2.1. The model

The model of the transmission system that we wish to analyse is depicted in Fig. 2. The cable is represented by the transfer function $H(f)$. Assume that the frequency interval of interest is such that the attenuation law is completely controlled by skin effect. Thus

$$|H(f)|^2 = \exp\{-kf^{1/2}\} \tag{1}$$

The constant k in eqn. (1) depends on the dimensions and the material of the cable and is given by

$$k = l\left(\frac{1}{r_0}+\frac{1}{r_1}\right)\left(\ln\frac{r_0}{r_1}\right)^{-1}\left(\frac{\pi\epsilon}{\sigma}\right)^{1/2} \tag{2}$$

l = length of the cable
r_0 = inside radius of the outer conductor
r_1 = radius of the inner conductor
ϵ = permittivity of the dielectric
σ = conductivity of the conductor material

To the output of the cable section is added white Gaussian noise with one-sided spectral density N.

Finally there is the signal power P at the input to the system. This signal power P is distributed over the frequency range of interest. If $p_i(f)$ is the

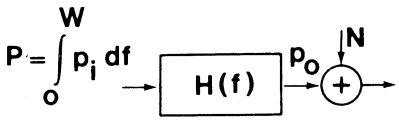

Fig. 2. The model of a single transmission link using a coaxial cable with transfer function $H(f)$.

power spectral density of the input signal and p_0 (f) the power spectral density of the output signal, there exists the relation

$$p_0(f) = p_i(f)|H(f)|^2 \tag{3}$$

Substituting eqn. (1) into eqn. **(3)** we obtain

$$p_i(f) = p_0(f) \exp\{kf^{1/2}\} \tag{4}$$

The input power P is given by

$$P = \int_0^\infty p_i(f)\,df = \int_0^\infty p_0(f) \exp\{kf^{1/2}\}\,df \tag{5}$$

The channel capacity is given by

$$C = \int_0^\infty \ln\left(1 + \frac{p_0(f)}{N}\right) df \tag{6}$$

2.2. The optimum input- and output spectral densities

To maximize the channel capacity C, it is necessary to distribute the signal power P in the proper way over the frequency range of interest. We therefore determine the function p_0 (f) and, related to this, p_i (f) in such a way that the channel capacity as given in eqn. (6) is a maximum under the constraint of a constant input power P. This isoperimetric problem can be solved by considering the integral

$$I = \int_0^\infty \ln\left(1 + \frac{p_0(f) + \epsilon g(f)}{N}\right) df - \lambda^{-1} \int_0^\infty \{p_0(f) + \epsilon g(f)\} \exp\{kf^{1/2}\}\,df \tag{7}$$

where $g(f)$ is an arbitrary function of f which is continuous and whose derivative is continuous in the range of integration; ϵ is a small quantity and λ^{-1} is a Lagrange multiplier to be determined for maximum channel capacity, which is done in the next section.
Differentiation of eqn. (7) yields:

$$\frac{dI}{d\epsilon} = \int_0^\infty \frac{1}{1 + \dfrac{p_0(f) + \epsilon g(f)}{N}} \frac{g(f)}{N}\,df - \lambda^{-1} \int_0^\infty g(f) \exp\{kf^{1/2}\}\,df \tag{8}$$

For $\epsilon = 0$ in eqn. (8) we have

$$\left(\frac{dI}{d\epsilon}\right)_{\epsilon=0} = \int_0^\infty \frac{g(f)}{N + p_0(f)}\,df - \lambda^{-1} \int_0^\infty g(f) \exp\{kf^{1/2}\}\,df \tag{9}$$

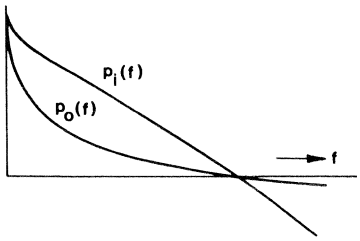

Fig. 3. Sketch of typical functions $p_0(f)$ and $p_i(f)$ according to eqns. (11) and (12)

The condition for a stationary value of the capacity under the stated constraint is

$$\left(\frac{dI}{d\epsilon}\right)_{\epsilon=0} = 0 \tag{10}$$

Combining eqns. (9) and (10) yields a formal condition for the power spectral density of the output signal

$$p_0(f) = h \exp\{-kf^{1/2}\} - N \tag{11}$$

Substituting eqn. (11) into eqn. (4) we have

$$p_i(f) = h - N \exp\{kf^{1/2}\} \tag{12}$$

Fig. 3 sketches the form of $p_0(f)$ and $p_i(f)$. It can be seen that these functions are both monotonically decreasing with increasing f.

For values of $kf^{1/2}$ greater that ln h/N they are both negative. However, a power density function must be non-negative, and therefore, if the input power P is assumed to be finite, an optimum power density function, with maximum channel capacity as a criterion, must be zero for frequencies higher than a certain finite frequency W and thus the upper limits of the integrals in eqn. (7) can be replaced by W. Obviously this change of the integration intervals has no influence on the results eqns. (11) and (12) insofar as the frequency interval from 0 to W is concerned. Thus

$$p_0(f) = \lambda \exp\{-kf^{1/2}\} - N \geqslant 0 \quad \text{for} \quad 0 \leqslant f \leqslant W \tag{13}$$

$$p_0(f) = 0 \quad \text{for all f} > W$$

$$p_i(f) = \lambda - N \exp\{kf^{1/2}\} \geqslant 0 \quad \text{for} \quad 0 \leqslant f \leqslant W \tag{14}$$

$$p_i(f) = 0 \quad \text{for all f} > W$$

From eqns. (13) and (14) we have

$$\lambda \geqslant N \exp\{kW^{1/2}\}$$

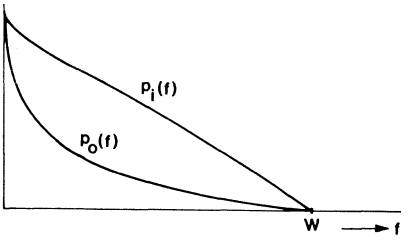

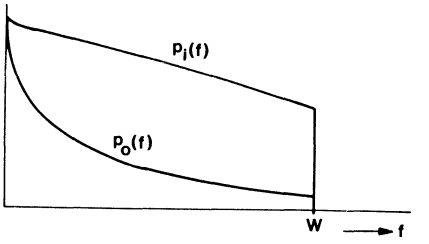

Fig. 4. Curves of the input and output power density functions according to eqns. (13), (14) and (16) with $W = 4/k^2$ and $a = 1$.

Fig. 5. Curves of the input and output power density [unctions according to eqns. (13), (14) and (16) with $W = 4/k^2$ and a = 2.

Or

$$\lambda = aN \exp\{kW^{1/2}\} \text{ for } a \geqslant 1 \tag{16}$$

Figs. 4 and 5 sketch the behavior of p, (f) and p_0 (f) with a = 1 and with a > 1 respectively.

In the appendix it is proven that with a given input power P the distribution of power must be as in Fig. 4, namely with a = 1 to obtain the maximum channel capacity.

2.3. The optimum channel capacity

For optimum channel capacity we have

$$\lambda = N \exp\{kW^{1/2}\} \tag{17}$$

Substituting eqn. (17) into eqn. (14) we obtain

$$p_i(f) = N\{\exp(kW^{1/2}) - \exp(kf^{1/2})\} \quad \text{for} \quad 0 \leqslant f \leqslant W \tag{18}$$

$$p_i(f) = 0 \quad \text{for all } f > W$$

Substituting eqn. (18) into eqn. (5) we get

$$P = N \int_0^W \{\exp(kW^{1/2}) - \exp(kf^{1/2})\}\, df$$

$$= NW \exp(kW^{1/2}) \left\{1 - \frac{2}{kW^{1/2}} + \frac{2}{k^2 W}\right\} - \frac{2N}{k^2} \tag{19}$$

Substituting eqn. (17) into eqn. (13) we have

$$p_0(f) = N[\exp\{k(W^{1/2} - f^{1/2})\} - 1] \quad \text{for} \quad 0 \leqslant f \leqslant W \tag{20}$$

$$p_0(f) = 0 \quad \text{for all } f > W$$

The maximum channel capacity is derived by substituting eqn. (20) into eqn. (6)

$$C = \int_0^W k(W^{1/2} - f^{1/2})\,\mathrm{d}f = \tfrac{1}{3}kW^{3/2} \tag{21}$$

Recapitulating, an optimum distribution of the available input power P with maximum channel capacity as a criterion includes a restriction to a baseband W of the cable. The value of W increases with the available input power and is given implicitly in eqn. (19). The power spectral density functions follow from eqns. (18) and (20) and the maximum channel capacity from eqn. (21).

2.4. Example

Assume the coaxial cable 1.2/4.4 mm (recommendation G.342 of the C.C.I.T.T.) with $r_1 = 0.6$ mm and $r_2 = 2.2$ mm. Applying formula (2) yields:

$$k = l\left(\frac{2}{1.2} + \frac{2}{4.4}\right) 10^3 \left(\ln \frac{4.4}{1.2}\right)^{-1} \left(\frac{\pi\epsilon}{\sigma}\right)^{1/2} \tag{22}$$

With $\epsilon = \epsilon_0\epsilon_r$ and $\epsilon_0 = \dfrac{10^{-9}}{36\pi}$; $\quad \epsilon_r \simeq 1.23$;

$$\sigma = 5.8 \times 10^{+7}\ \Omega^{-1}\mathrm{m}^{-1}; \quad k = 1.25 \times 10^{-6}\, l. \tag{23}$$

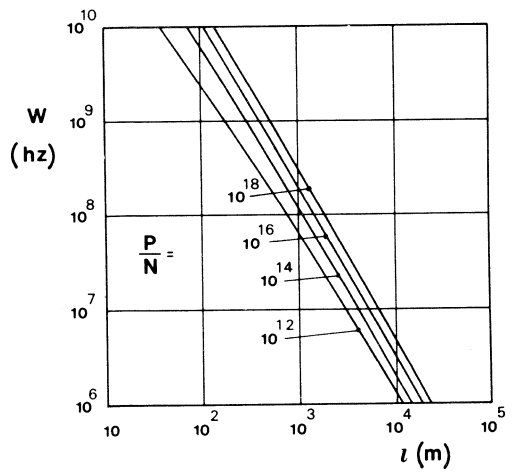

Fig. 6. The optimum bandwidth of a coaxial cable 1.2/4.4 mm as a function of the length l and with different values of P/N.

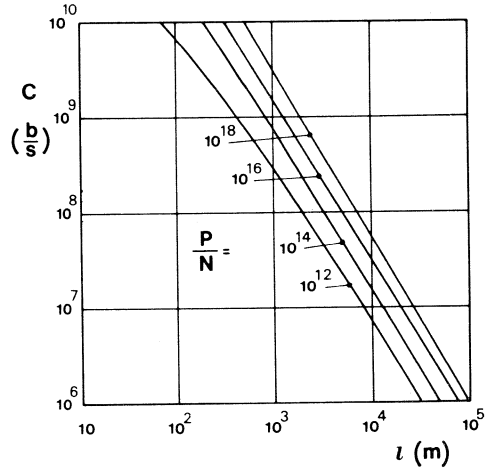

Fig. 7. The channel capacity of a coaxial cable 1.2/4.4 mm as a function of the length l for different values of P/N.

This theoretical value is in close agreement with a measured value of the attenuation of this type of cable at a frequency of 10^9 Hz that shows 17.2 dB for a length of 100 m.

Formulae (19) and ***(23)*** give implicitly tht relation between W and 1 with P/N a parameter. And with eqn. (21) the channel capacity can be calculated. Fig. 6 shows the bandwith W as a function of the length with P/N a parameter and Fig. 7 shows the channel capacity C as a function of the length 1 of the cable.

3. The maximum channel capacity of a multiwire cable

As mentioned in the introduction, an n-wire cable can be used to form n independent communication channels by taking advantage of the n independent transmission modes in one direction. We will call such an independent channel a subchannel. Thus the communication channel that can be formed with a multiwire cable consists of a set of n subchannels, each subchannel associated with a particular transmission mode. The model that we will use to derive the maximum channel capacity of a multiwire cable consists therefore of a set of n submodels as depicted in Fig. 8.

Each particular subchannel has its own transfer function that is determined by the attenuation and dispersion of the transmission mode with which this subchannel is associated. Again we will assume that the transfer functions are completely controlled by skin effect, so that the square of the modulus of the transfer function of the j-th subchannel can be described by:

$$|H_j(f)|^2 = \exp\{-k_j f^{1/2}\} \tag{24}$$

with k_j a constant that depends on the dimensions and the material of the cable and on the transmission mode j.

For the sake of simplicity we will assume equal noise power densities N for the different subchannels, a reasonable assumption if we think of equal temperatures of the conductors and equal noise figures for the amplifiers used.

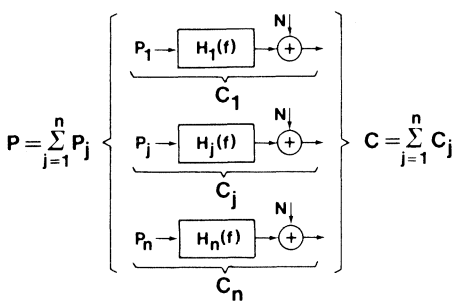

Fig. 8. The model used to calculate the channel capacity of a multiwire cable with n parallel conductors in a shield.

As we want to compare the performance of an n-wire cable with the performance of a coaxial cable, the latter being a special case of the former with n = 1, we assume the total available power for a length l of the cable to be constant, independent of n and denote it by P. This power P is subdivided into n parts and each part P_j is used for the particular subchannel j. Thus:

$$P = \sum_{j=1} P_j \tag{25}$$

In agreement with eqn. (21) we find, for the maximum channel capacity of subchannel j:

$$C_r = \tfrac{1}{3} k_r W_j^{2/3} \tag{26}$$

with W, given implicitly by:

$$P_j = NW_j \left(1 - \frac{2}{k_j W_j^{1/2}} + \frac{2}{k_j^2 W_j}\right) \exp\{k_j W_j^{1/2}\} - \frac{2N}{k_j^2} \tag{27}$$

which is in accordance with eqn. (19). The noise sources being uncorrelated, the channel capacity of the multiwire cable is the sum of the n subchannel capacities that are related to the n independent transmission modes. Thus:

$$C = \sum_{j=1} C_j \tag{28}$$

As C_j is a function of P_j, C is a function of the n powers P_j.

We now determine the distribution of power over the different subchannels that results in maximum C by using Lagrange's method of undetermined multipliers. A necessary condition for an extremum of C under the constraint of constant total power P is:

$$\text{grad } (C + \lambda P) = \underline{0} \tag{29}$$

with λ a Lagrange multiplier.

Because C_j is only a function of the power P_j and because $\partial P/\partial P_j = 1$ the condition (29) reduces to:

$$\frac{\partial C_j}{\partial P_j} + \lambda = 0 \quad j = 1, \ldots, n \tag{30}$$

Differentiation of eqns. (26) and (27) to the common parameter W_j yields

$$\frac{dC_j}{dW_j} = \tfrac{1}{2} k_j W_j^{1/2} \tag{31}$$

and

$$\frac{dP_j}{dW_j} = \tfrac{1}{2} N k_j W_j^{1/2} \exp\{k_j W_j^{1/2}\} \tag{32}$$

respectively.

Combination of eqns. (31) and (32) gives:

$$\frac{dC_j}{dP_j} = \{N \exp(k_j W_j^{1/2})\}^{-1} \tag{33}$$

With eqn. (33) the condition (30) reads:

$$k_j W_j^{1/2} = \text{constant} = K \tag{34}$$

In practical situations the term $\frac{2N}{k_j^2}$ in eqn. (27) can be neglected.

Combination of eqns. (34) and (27) then results in:

$$P_j = \frac{N}{k_j^2}(K^2 - 2K + 2) \exp\{K\} \tag{35}$$

Combination of eqns. (34) and (26) gives:

$$C_j = \tfrac{1}{3} k W_j^{3/2} \tag{36}$$

4. Computational results

The calculations are based on the analysis by H. Kaden of cables of the kind considered in this paper [10]. He gives, in the reference cited, formulas for the attenuation of the different modes in 2-wire and 4-wire cables.

From eqn. (1), it follows that the relation between the constant k_j and the related attenuation per unit of length a, of the exited mode is given by:

$$k_j = \frac{2\alpha_j l}{\sqrt{f}} \tag{37}$$

To be able to compare the properties of interest of cables with different numbers of inner conductors, we will compare cables with equal outer conductors. To that end suppose first a coaxial cable with an outer conductor of inside radius r_0 and an inner conductor of radius r,. Assume a ratio 3.6 between the radii of these conductors to obtain a cable with minimum attenuation and consequently maximum channel capacity, given r_0. Assume further:

$$r_0 = 5 \text{ mm}$$

$$\sigma = 5.8 \times 10^7 [\Omega \text{m}]^{-1}$$

$$\frac{P}{N} = 10^{18} \text{ s}^{-1}$$

$$\epsilon_r = 2.36 \tag{38}$$

The constant k that determines the transfer function of the coaxial cable fol-

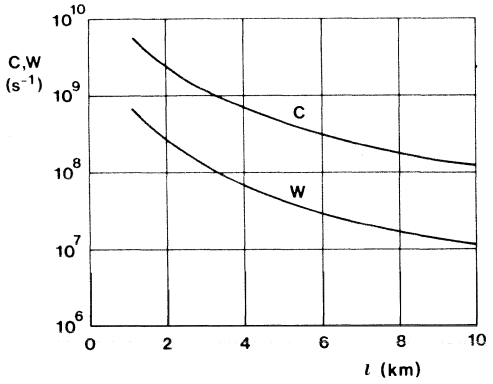

Fig. 9. The maximum channel capacity C of a coaxial cable and the related bandwidth W as a function of the length l. $r_0 = 0.5 \times 10^{-2}$ m, $P/N = 10^{18}$ x s^{-1}, $\sigma = 5.8 \times 10^7$ $[\Omega m]^{-1}$ and $\epsilon_r = 2.36$.

lows from eqns. (2) and (38):

$$k = 7.64 \times 10^{-7}\, l \tag{39}$$

The bandwidth W and the maximum channel capacity C are calculated from eqns. (19) and (21) respectively and plotted in Fig. 9 as functions of the length l.

Next we consider a 2-wire cable with the same inside radius of the outer conductor as in the previous case. The two independent subchannels are characterized by their transfer functions, which in turn are determined by the k_j's ($j = 1,2$). The constants k_j follow from eqn. (37). The attenuations α_j can be expressed in r„ r_2 and a, the dimensions that describe the cross-section of the cable being as depicted in Fig. 10. Following [10] we derive:

$$k_1 = 9.91 \times 10^{-7}\, l$$

$$k_2 = 11.92 \times 10^{-7}\, l \tag{40}$$

If k_1 and k_2 are known, P_j can be calculated from eqns. (25) and (35) and thereupon k, W_j, C_j and C follow respectively from eqns. (35), (34), (36) and (28).

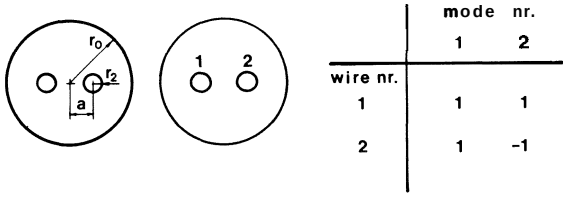

Fig. 10. The cross-section of the optimum 2-wire cable and the way in which the conductors must be excited to form the subchannels. $r_0 = 5$ mm; a = 1.8 mm; $r_2 = 0.81$ mm.

Obviously, the channel capacity C thus calculated is a function of r_2 and a. The values of r_2 and a that make C a maximum can be determined and appear to be:

$$r_2 = 0.162\, r_0$$

$$a = 0.36\, r_0 \tag{41}$$

The resulting cross-section, as well as the way in which the conductors must be excited to form the subchannels, is depicted in Fig. 10. The maximum channel capacity C as a function of the length l of the cable, assuming the same P/N, a and ϵ_r as in the previous case of the coaxial pair, is plotted in Fig. **11.** It is the sum of the two maximum subchannel capacities $C_1 = C_c$ and $C_2 = C_d$ belonging to the channels formed by the common mode and the differential mode. These subchannel capacities and the corresponding bandwidths $W_1 = W_c$ and $W_2 = W_d$ are also plotted in Fig. **11.**

Note that (a) the maximum channel capacity of the 2-wire cable practically equals the maximum channel capacity of the coaxial cable; (b) the highest frequency W_1 is substantially lower than the frequency W for the coaxial cable; (c) the total mass of the copper used for the inner conductors is 68% of the mass of the copper needed for the inner conductor of the coaxial cable.

Finally we consider a 4-wire cable. Again following [10] we derive the four k_j's:

$$k_1 = 1.11 \times 10^{-6}\, l$$

$$k_2 = k_3 = 1.27 \times 10^{-6}\, l$$

$$k_4 = 1.16 \times 10^{-6}\, l \tag{42}$$

In the same way as was done in the case of the 2-wire cable, we can calculate

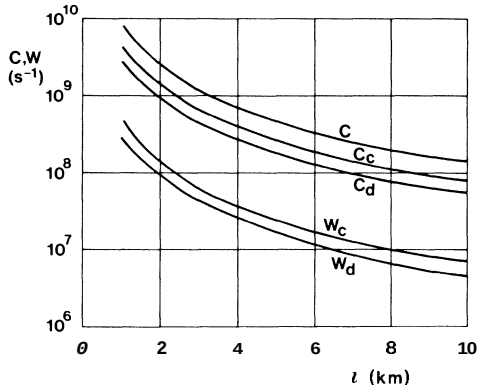

Fig. 11. The maximum channel capacity of the 2-wire cable, together with the maximum subchannel capacities C_c and C_d and the related bandwidths W_c and W_d as functions of the length l of the cable. The subscripts c and d stand for the common and differential mode respectively.

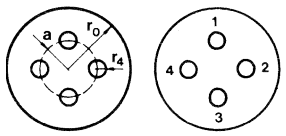

	mode nr			
	1	2	3	4
wire nr.				
1	1	1	0	1
2	1	0	1	-1
3	1	-1	0	1
4	1	0	-1	-1

Fig. 12. The cross-sextion of the optimum 4-wire cable ancl the way in which the conductors must be excited to form the subchanneis. r_0 = 5 mm; a = 2.3 mm and r_4 = 0.69 mm.

$P_{,}$, K, W_j, C_j and C. For maximum C it follows that r_4 and a are given by:

$$r_4 = 0.138\, r_0$$

$$a = 0.46\, r_0 \tag{43}$$

resulting in a cross-section as depicted in Fig. 12. The way to form the subchannels is also given in this figure.

The maximum channel capacity C is plotted in Fig. 13. It is again the sum of the four subchannel capacities C_1—C_4. These as well as the corresponding W_1—W_4 are also plotted in Fig. 13.

Note that (a) the maximum channel capacity of the 4-wire cable is substantially higher than the maximum channel capacity of the coaxial cable; (b) the highest frequency W_1 is lower than the frequency W for the coaxial cable and the frequency W_1 for the 2-wire cable; (c) the total mass of the copper for the four inner conductors equals the mass of the copper needed for the inner conductor of the coaxial cable.

We now illustrate by an example the performance of the different cables

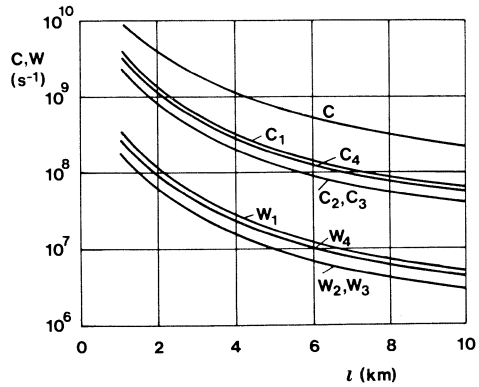

Fig. 13. The maximum channel capacity of the 4-wire cable, together with the maximum subchannel capacities C_1—C_4 and the related bandwidths W_1—W_4 as functions of the length l of the cable.

described. Assume that a digital transmission system has to be built for a bit rate of 300 Mb/s and with PIN = 10^{18} s^{-1}. With the ideal combination of encoder, cable and decoder we can make the distance between neighbouring repeaters with the coaxial and with the 2-wire cable 6300 m. The 4-wire cable can span a distance of 8100 m.

The highest frequencies used are, respectively, 26, 15.5 and 7.5 MHz. The quantities of copper for the inner conductor of the coaxial cable and the conductor pair of the 2-wire cable are 340 and 230 kg respectively for a single span.

5. Conclusion and remarks

With the channel capacity as a criterion, it can be advantageous to replace the single inner conductor of a coaxial cable by two or more conductors. Specifically, if the single conductor is replaced in the described manner by two conductors, there results a saving of copper and if four conductors are used, there results an appreciable higher channel capacity. A further advantage is that an increase in the number of conductors results in a decrease of the bandwidth, which implies simpler hardware.

The results derived in this paper suggest one might also investigate cables with n = 3, 5, 6, etc.

Analysis shows that a digital system for a coaxial pair should use a large number of levels to be optimum in the sense of maximum bit rate under the constraint of constant bit error probability [9,11]. This large number of levels, with its inherent technical and economical problems can be evaded by using an n-wire cable with parallel conductors instead of a coaxial cable. For instance instead of using a coaxial cable and 16 levels, one could use the 4 independent channels of a 4-wire cable, each particular channel having two levels.

If n-wire cables are applied in P.C.M. systems, it is possible to match the channels in the sense of their capacities to the significance of the bits; the channel with the highest capacity can be used for the most significant bit and so on.

Systems, realized with the n-wire cables, can be treated as multichannel systems that are the subject of several papers on multichannel communication theory [12].

References

1 J.R. Carson and R.S. Hoyt, Propagation of periodic currents over a system of parallel wires, Bell Syst. Tech. J., 6 (1927) 495.

2 L.A. Pipes, Matrix theory of multiconductor transmission lines, Philos. Mag., 24 (1937) 97.

3 H. Ameniya, Time-domain analysis of multiple parallel transmission lines, RCA Rev., 28 (1967) 241.

4 D.A. Shnidman, A generalized Nyquist criterion and an optimum linear receiver for a pulse modulation system, Hell Syst. Tech. J., 46 (1967) 2163.
5 W. van Etten, An optimum linear receiver for multiple channel digital transmission systems, IEEE Trans. Commun., 23 (1975)828.
6 C.E. Shannon, Communication in the presence of noise, Proc. IRE, 37 (1949)10.
5 T. Berger and D.W. Tufts. Optimum pulse amplitude modulation. Part 1: Transmitter-receiver design and bounds from information theory, IEEE Trans. Inf. Theory. 13 (1967)196.
8 G. Raisbeck, Optimal distribution of signal power in a transmission link whose attenuation is a function of frequency, IRE PGIT Trans., 4 (1958) 129.
9 J.R. Pierce, Information rate of a coaxial cable with various modulation systems, Hell Syst. Tech. J., 45 (1966)1197.
10 H. Kaden, Wirbelströme und Schirmung in der Nachrichtentechnik. Springer-Verlag, Berlin-Göttingen-Heidelberg, 1959.
11 A.J. Gibs, Digital capacity of standard coaxial pair, report number 6647, Research Laboratories Australian Post Office, March 1973.
12 A.D. Wyner, Recent results in the Shannon Theory, IEEE Trans. Inf. Theory, 20 (1974) 2.

Appendix

In this appendix we prove that for maximum channel capacity the equality sign in eqns. (15) and (16) must be chosen. To do so, we consider two different ways to distribute an equal amount of input power over the frequency hand as depicted in Fig. A.1.

In the first place we assume

$$\lambda = N \exp\{kW_1^{1/2}\} \tag{A.1}$$

that has associated with it an input power P_1 and a channel capacity C_1 corresponding respectively with eqns. (19) and (21)

$$P_1 = NW_1\left(1 - \frac{2}{kW_1^{1/2}} + \frac{2}{k^2W_1}\right) \exp\{kW_1^{1/2}\} - \frac{2N}{k^2} \tag{A.2}$$

$$C_1 = \tfrac{1}{3}kW_1^{3/2} \tag{A.3}$$

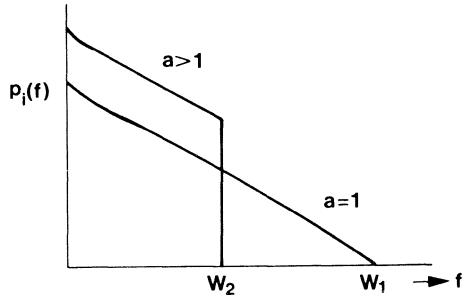

Fig. A.1. Two different ways of input power frequency distribution.

In the second place we assume

$$\lambda = aN \exp\{hW_2^{1/2}\} \quad \text{with a} > 1 \tag{A.4}$$

Substituting eqn. (A.4) into eqn. (14) we have the power spectral density of the input signal in this second case

$$p_i(f) = N\{a \exp(kW_2^{1/2}) - \exp(kf^{1/2})\} \quad \text{for } 0 \leqslant f \leqslant W, \tag{A.5}$$

$$p_i(f) = 0 \quad \text{for all f} > W,$$

Substituting eqn. (A.5) into eqn. (5) we obtain the input power

$$P_2 = NW_2\left(a - \frac{2}{kW_2^{1/2}} + \frac{2}{k^2W_2}\right) \exp\{kW_2^{1/2}\} - \frac{2N}{k^2} \tag{A.6}$$

Substituting eqn. (A.4) into eqn. (13) we get

$$p_0(f) = aN \exp(kW_2^{1/2} - kf^{1/2}) - N \quad \text{for } 0 \leqslant f \leqslant W_2 \tag{A.7}$$

$$p_0(f) = 0 \quad \text{for all f} > W_2$$

And substituting eqn. (A.7) into eqn. (6) we have

$$C_2 = \tfrac{2}{3}kW_2^{3/2} + W_2 \ln a \tag{A.8}$$

The condition for equal power in both cases is

$$P_1 = P_2 \tag{A.9}$$

If we introduce for the sake of simplicity the notation

$$b = W_1^{1/2}W_2^{-1/2} \quad \text{and} \quad x = kW_2^{1/2} \tag{A.10}$$

the condition (A.9) reads

$$a = \left(b^2 - \frac{2b}{x} + \frac{2}{x^2}\right) \exp\{(b-1)x\} + \frac{2}{x} - \frac{2}{x^2} \tag{A.11}$$

It is clear from eqn. (A.11) that the requirement a > 1 as stated in eqn. (A.4) implies

$$b > 1 \tag{A.12}$$

Eliminating W_1 from eqns. (A.3) and (A.10) we obtain

$$C_1 = \tfrac{1}{3}kW_2^{3/2} + \frac{b^3-1}{3}kW_2^{3/2} \tag{A.13}$$

Comparing eqns. (A.8) and (A.13) we see that $C_1 > C_2$ iff

$$a < \exp\left\{\frac{b^3-1}{3}x\right\} \tag{A.14}$$

To show the validity of eqn. (A.14) we expand the exponent in eqn. (A.11)

in a power series yielding

$$a = \left(b^2 - \frac{2b}{x} + \frac{2}{x^2}\right)\left\{1 + (b-1)x + \ldots \frac{(b-1)^n x^n}{n!} + \ldots\right\} + \frac{2}{x} - \frac{2}{x^2}$$

$$= 1 + \sum_{n=1}^{\infty}\left(\frac{b^2(b-1)^n}{n!} - \frac{2b(b-1)^{n+1}}{(n+1)!} + \frac{2(b-1)^{n+2}}{(n+2)!}\right)x^n$$

$$= 1 + \sum_{n=1}^{\infty} \frac{(b-1)^n}{n!} \cdot \frac{n(n+1)b^2 + 2nb + 2}{(n+1)(n+2)} \cdot x^n \tag{A.15}$$

Expanding the right hand side of eqn. (A.14) in a power series, we have

$$\exp\left\{\frac{b^3-1}{3}x\right\} = 1 + \sum_{n=1}^{\infty} \frac{(b-1)^n}{n!} \cdot \frac{(b^2+b+1)^n x^n}{3} \tag{A.16}$$

Taking the difference between eqns. (A.16) and (A.15) we get

$$\exp\left\{\frac{b^3-1}{3}x\right\} - a = \sum_{n=2}^{\infty} \frac{(b-1)^n}{n}\left[\frac{(b^2+b+1)^n}{3} - \frac{n(n+1)b^2 + 2nb + 2}{(n+1)(n+2)}\right]x^n \tag{A.17}$$

Noting that

$$\frac{(b^2+b+1)^n}{3} = \frac{\text{sum of positive terms} + n(n+1)b^2 + 2nb + 2}{6} \tag{A.18}$$

we conclude that every term in the sum (A.17) is positive so the sum is positive and (A.14) is proved. Therefore the first method of distributing the input power is the one that leads to a maximum channel capacity.

Journal of Applied Science of Engineering A, 2 (1977) 141 153

POWER SYSTEM IDENTIFICATION IN THE POWER FLOW REFERENCE FRAME

K.I. DENNO

New Jersey Institute of Technology, Newark, N J (U S A)

(Received June 33, 1976, in revised form February 25, 1977)

Summary

This paper presents a procedural method for selecting and designing an acceptable optimum power system configuration from a group of system alternatives, to be established in a single area or multiarea mode.

The procedural method developed is based on compiling data obtained from load flow calculations with that of the optimum transmission loss coefficients matrix [B] for each system, to come up with an optimum design of any power system network in the sixth reference frame.

Identification of the optimum power network is in terms of the symmetrical resistance matrix as indicated in the following equation:

$$[R] = [K]\ [B]^{-1} \qquad (0)$$

where

[R] is the symmetric resistance matrix
[B] is the optimum transmission loss coefficients matrix
[K] is a matrix function of load flow calculation parameters

By inspection of the [R] matrices for a group of optimum power system alternatives, established under various percentages of total load received, the most economically-optimum system can be identified, and a series of matrix transformations produce its form in the actual or first reference frame.

Load flow calculations using the Newton—Raphson method and power system optimization have been applied on 23,000-MW capacity of a centralized and a mixed centralized-dispersed power systems under all loadings to calculate the [K] and the optimum [B] matrices, respectively. Then by eqn. (0) above, elements of the [R] matrices reflecting power system representation in the power flow frame have been established for all systems and subsytems, from which the most economically-optimum power network is

selected relying on the elements of the diagonal [R] matrices, since they represent the direct path from each equivalent power source to the system centroid.

it can be stated that analyzing any arbitrary power system in the power flow reference frame according to the method presented in this paper can be very economical with respect to consumption of computer time and memory, since in this frame, there is a substantially smaller number of total power busbars and branches than in the actual power network.

1. Introduction [1–4]

Electrical power systems are generally represented in conventional form in terms of data related to actual generating sources, loads and impedances of the interconnecting network. This is the first reference frame as called by G. Kron. On the other hand, engineers in a single power area and multiarea power pool usually deal with real power of the generating sources and real power exchange.

In situations where prompt and decisive action is needed in comparing several power systems of different configurations under a unified constraint, it becomes necessary that those systems be expressed and identified in an overall power equivalent reference frame. Also, the calculation of economic scheduling of generation which relates the generating capacity of individual plants to total generation based on coordinating incremental production costs and incremental transmission losses, is carried out in the power flow reference frame (the sixth reference frame as called by G. Kron).

Optimization of power systems from an economic standpoint can proceed on the basis of arbitrary interconnecting networks in the power flow reference frame subject to certain constraints such as minimum losses, specified total generation, specified plant capacity and total received load.

Determination of the optimum power system network in the sixth or power flow reference frame can be followed by a series of transformations aimed at representing the optimum system in the actual or first reference frame. To compare and analyze from the start several power system alternatives in the actual first reference frame requires excessive computer time as well as large memory capacity to absorb all the data.

The foregoing points out the necessity to develop a criterion by which power system optimization in the power flow reference frame can be carried out using the [B] matrix, power source outputs within their maximum ranges, and fuel cost data. Such a criterion was developed earlier [2] and treated successfully on small power systems.

Based on the solution obtained for the optimum B matrix, coupled with data from load flow calculation, a new path for designing the power network in the sixth or power flow reference frame will be developed and tested in this paper.

2. Statement of the problem

Given several optimum power system configurations to be established in a single area or multiarea mode, with each system follows the conditions:

(*a*) The system contains *n* equivalent generating sources of electromechanical, electrochemical, solar, thermionic and nuclear nature, each possessing a prescribed fuel cost curve, as shown in Fig. **1.**

(*b*) Each system operates optimally according to the coordination criteria relating incremental. generation costs and incremental transmission losses costs, as expressed by eqn. **(1)**

$$\frac{\partial F_i}{\partial P_i} + \lambda \frac{\partial P_L}{\partial P_i} = \lambda \tag{1}$$

where

λ = incremental cost of received power in dollars per MW-h
P_i = power generating capacity of plant i in MW
F_i = fuel cost of plant i in dollars per hour
P_L = total transmission losses

The coordination eqn. **(1)** is subject to the following constraints:

$$\phi(P_1, P_2 \ldots P_n) = \sum_{i=1}^{n} P_i - P_r - P_L = 0 \tag{2}$$

$$P_L \cong \sum_i \sum_j P_i B_{ij} P_j \tag{3}$$

where

P_r = given received power (load)
B_{ij} = elements of the transmission loss matrix

The [B] matrix is assumed an implicit function of all power sources as indicated in eqns. (5) and (6) below.

$$P_j = f(P_i) \tag{4}$$

$$B_{ij} = g(P_i) \tag{5}$$

Eqns. (4) and (5) imply general recognition that B_{ij} is strongly connected

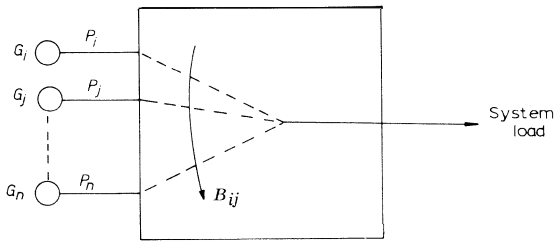

Fig. 1. Power flow reference frame.

to power transfers among generating sources.

Because B_{ij} is considered here an implicit function of power sources, hence the total transmission loss P_L is assumed to take the functional form:

$$P_L = \sum_i \sum_j P_i B_{ij} P_j \text{ or,} \tag{6}$$

$$= \psi(P_i, B_{ij}, P_j) \tag{7}$$

The problem centers on obtaining the optimum power system representation in the power flow reference frame in terms of the symmetrical resistance matrix. The solution will be verified on two systems, namely:

(1) A totally centralized system with electromechanical and electrochemical generating units.

(2) A mixed dispersed-centralized system with electrochemical and electromechanical generating units.

3. Optimal solution for the [B] matrix [1,2,4]

Rewrite eqn. (1):

$$\frac{\partial F_i}{\partial P_i} + \lambda \frac{\partial P_L}{\partial P_i} = \lambda$$

and assuming that a general functional form for the incremental fuel cost curve for the power generating sources is linear, such that

$$\frac{\partial F_i}{\partial P_i} = F_{ii} P_i + f_i \tag{8}$$

where

$\frac{\partial F_i}{\partial P_i}$ = incremental fuel cost of plant i in dollars/MW-h

F_{ii} = slope of incremental fuel cost surve

f_i = incremental cost of plant i at zero output,

Substituting in eqn. (1) from eqns. (6) and (8) together with the limitation of dependence stated in eqns. (4) and (5), the following partial differential equation is obtained:

$$F_{ii} P_i + f_i + \lambda \left[B_{ij} P_j + \frac{\partial P_L}{\partial P_j} \frac{\partial P_j}{\partial P_i} + \frac{\partial P_L}{\partial B_{ij}} \frac{\partial B_{ij}}{\partial P_i} \right] = \lambda \tag{9}$$

Eqn. (9) can be written as

$$F_{ii} P_i + f_i + \lambda \left[B_{ij} P_j + P_i B_{ij} \frac{dP_j}{dP_i} + P_i P_j \frac{dB_{ij}}{dP_i} \right] = \lambda \tag{10}$$

where

P,, B_{ij} and P_i are symmetrical matrices.

Similarly. a compatible partner to eqn. (10) is found and expressed below:

$$F_{jj}P_j + f_j + \lambda\left[P_iB_{ij} + B_{ij}P_j\frac{\mathrm{d}P_i}{\mathrm{d}P_j} + P_iP_j\frac{\mathrm{d}B_{ij}}{\mathrm{d}P_j}\right] = \lambda \tag{11}$$

Eqns. (10) and (11) are two compatible matrix differential equations, written in different functional forms in eqns. (12) and (13), respectively:

$$\eta\left(P_i, P_j, B_{ij}, \frac{\partial B_{ij}}{\partial P_i}, \frac{\partial B_{ij}}{\partial P_j}\right) = 0 \tag{12}$$

$$\tau\left(P_i, P_j, B_{ij}, \frac{\partial B_{ij}}{\partial P_i}, \frac{\partial B_{ij}}{\partial P_i}\right) = 0 \tag{13}$$

$\therefore$

$$\eta - \tau = \xi = 0 \tag{14}$$

Eyn. (14) is another compatible differential equation, which can be solved for Pi, P_j, B_{ij}, $\delta B_{ij}/\delta P_i$ and $\delta B_{ij}/\delta P_j$ by conversion to a canonical system, presented below:

$$\frac{\mathrm{d}P_i}{\mathrm{d}\xi_{P_i}} = \frac{\mathrm{d}P_j}{\mathrm{d}\xi_{P_j}} = \frac{-\mathrm{d}Q}{\xi_{P_j} + Q\xi_{B_{ij}}} = \frac{-\mathrm{d}Z}{\xi_{P_i} + Z\xi_{B_{ij}}} = \frac{\mathrm{d}B_{ij}}{Z\xi_Z + Q\xi_Q} \tag{15}$$

where

$$Z = \frac{\partial B_{ij}}{\partial P_i},\ Q = \frac{\partial B_{ij}}{\partial P_j}$$

$$\xi_{P_i} = \frac{\partial \xi}{\partial P_i},\ \xi_{P_j} = \frac{\partial \xi}{\partial P_j},\ \xi_{B_{ij}} = \frac{\partial \xi}{\partial B_{ij}}$$

Apply eqn. (14) on eqn. (15) to obtain:

$$\frac{\mathrm{d}Z}{F_{ii}Q} = \frac{\mathrm{d}Q}{F_{jj}Z} \tag{16}$$

or

$$F_{jj}Z^2 + F_{ii}Q^2 = k^2 \tag{17}$$

k^2 is a constant

Expressions for Q and Z could be secured by solving simultaneously eqns. (10) and (11).

For the purpose of finding the constant k^2 in eqn. (17), the following boundary conditions are secured from eqn. (1),

$B_{ij} = 0$ for

$$P_i = \frac{\lambda - f_i}{F_{ii}} \tag{18}$$

and

$$P_j = \frac{\lambda - f_j}{F_{jj}} \tag{19}$$

$\therefore$ from eqn. (17), resulting that $k^2 = 0$

and now it becomes,

$$F_{jj}\left(\frac{\partial B_{ij}}{\partial P_i}\right)^2 + F_{ii}\left(\frac{\partial B_{ij}}{\partial P_j}\right)^2 = 0 \tag{20}$$

After solving simultaneously eqns. (10) and (11) for Q and Z, and then substituting in eqn. (20), the following solution for B_{ij} is obtained,

$$B_{ij} = [-F_{ii}F_{jj}P_iP_j + (\lambda F_{ii} - F_{ii}f_j)P_i + (\lambda F_{jj} - F_{jj}f_i)P_j + \\ + (\lambda f_i + \lambda f_j - f_i f_j - \lambda^2)]/[2\lambda F_{ii}P_i^2 + 2\lambda F_{jj}P_j^2 + \\ + (2\lambda f_i - 2\,\mathrm{h}^2)\mathrm{P_i} + (2\lambda f_j - 2\lambda^2)P_j] \tag{21}$$

The above solution for the [B] matrix is based on minimum cost for a given received load in terms of optimum scheduling of generation of all power sources and fuel cost data. Of course elements of the [B] matrix will change under different total received load with a new scheduling of generation.

4. Power flow reference frame *[3]*

Where all real powers are expressed in a frame involving power exchange among various equivalent generating sources as shown in Fig. *1*.

The matrix of transformation to the power flow or sixth reference frame is known as the loss matrix with general terms given below.

$$B_{ij} = K_{ij}R_{ij} - H_{ij}(f_i - f_j) \tag{22}$$

Then the total transmission loss P_L is expressed as:

$$P_L = \sum_i \sum_j P_i K_{ij} R_{ij} P_j - P_j H_{ij}(f_i - f_j)P_i \tag{23}$$

where

$$K_{ij} = \frac{1}{V_i V_j}\,[(1 + S_iS_j)\cos\phi_{ij} + (S_i - \mathrm{S},)\sin\phi_{ij}] \tag{24}$$

$$H_{ij} = \frac{1}{V_i V_j}\,[(1 + S_iS_j)\sin\phi_{ij} + (S_i - S_j)\cos\phi_{ij}] \tag{25}$$

$$f_i = R_{Gi-Lk}\, l_k \tag{26}$$

$$f_j = R_{Gj-Lk}\, l_k \tag{27}$$

$$l_k = i_{LK}/i_L \tag{28}$$

l_k = the ratio of load current at bus k to total load current
$R_{Gi\ Lk}$ = resistance between generator i and load k
$R_{Gj\ Lk}$ = resistance between generator j and load k
R_{ij} = symmetric resistance in the sixth frame
$H_{ij}(f_i - f_j$ = could he neglected in a power system where ϕ_{ij} and $(S_i - S_j)$ are small, respectively
S_i – ratio of reactive to real power at bus i
Φ_{ij} = phase angle between buses i and j, respectively

∴ Eqn. (11) becomes:

$$P_L = \sum_i \sum_j P_i K_{ij} R_{ij} P_j \tag{29}$$

or

$$B_{ij} \approx K_{ij} R_{ij} \tag{30}$$

$$R_{ij} = B_{ij} K_{ij}^{-1} \tag{31}$$

5. Basis for power system network in the power flow frame [1–3,5]

The design criterion for an optimum power system of an arbitrary interconnecting network subject to the constraints of minimum transmission losses, specified total received load, and specified plant capacity, is one of the objectives of this paper. Such a criterion is based on the calculation of the symmetrical resistance matrix in the power flow reference frame.

Also, a knowledge of the resistance matrices of more than one interconnecting network could serve as the basis for identifying the nature and type of the power system, *i.e.*, whether it be a centralized system, a dispersed system or a mixed centralized-dispersed system as far as the locations of the power generating sources are concerned.

The solution of the [B] matrix in terms of power generating sources within their capacity and fuel cost data was obtained and restated in eqn. (21) with the [K] matrix given in eqn. (24).

Eqn. (30) can be expanded in matrix form and written as follows:

$$\begin{bmatrix} B_{11}B_{12}\ldots B_{1n} \\ B_{21}B_{22}\ldots B_{2n} \\ B_{n1}B_{n2}\ldots B_{nn} \end{bmatrix} = \begin{bmatrix} (K_{11}R_{11})(K_{12}R_{12})\ldots(K_{1n}R_{1n}) \\ (K_{21}R_{21})(K_{22}R_{22})\ldots(K_{2n}R_{2n}) \\ (K_{n1}R_{n1})\ldots \qquad\qquad (K_{nn}R_{nn}) \end{bmatrix}$$

$$\therefore R_{11} = \frac{B_{11}}{K_{11}} \tag{32}$$

$$R_{12} = \frac{B_{12}}{K_{12}} \text{ and so on} \tag{33}$$

$$R_{nn} = \frac{B_{nn}}{KT,n}$$

6. Using the diagonal $[R]$ matrices in comparison of power system alternatives

The overall $[R]$ matrix can be expressed as below:

$$[R] = \begin{bmatrix} B_{11}/K_{11} \ldots B_{1n}/K_{1n} \\ B_{21}/K_{21} \ldots B_{2n}/K_{2n} \\ \\ B_{n1}/K_{n1} \ldots B_{nn}/K_{nn} \end{bmatrix} \tag{34}$$

The elements in the matrix of eqn. (34) are the self symmetrical resistances of the individual power sources from a reference point, and mutual symmetrical resistances among the individual sources, all represented in the power flow frame.

. R , $R_{22} \ldots R_{nn}$ = the self symmetrical resistance of power sources **1,** 2, **3,** ..., n with respect to a reference point.

$R_{12}, R \quad \ldots R_{1n}$ = the mutual symmetrical resistances between power source No. **1** with respect to power source No. n.

Calculation of the $[R]$ matrix elements requires the following data:

(1) Load flow calculations to secure information for the [K] matrix, namely voltage magnitude, phase angle, real and reactive power of each busbar.

(2) Complete establishment of the [B] matrices under all loadings for the presumed power system. (*i.e.* for every value of P,). Application of eqn. **(34)** together with the procedure of calculating the $[R]$ symmetric matrix which reflects an optimum power system design in the power flow reference frame, was demonstrated for the following two systems. As an example:

(A) A centralized system of 32 equivalent power source busbars with total peak received load of 23,000 MW.

(B) A dispersed-centralized system of 123 equivalent busbars having the same total peak received load of 23,000 MW.

For the above two presumed systems, load flow calculations were carried out on all loadings based on the Newton—Raphson method on the IBM 360 Computer.

Also the [B] matrices for all loadings were obtained for the above-mentioned two systems according to eqn. (21) where in each case P_r was taken at 60%, 7096, 80%, 90% and 100% of peak received load.

By compiling elements from the $[K]$ matrices with those of the $[B]$ matrices for the two systems, elements of the $[R]$ matrices are obtained by a simple computer program, run on the RCA 70 machine, the capacity

of which was quite adequate even for the large number of 123 busbars.

However, since the number of busbars in the centralized-dispersed system is 123, compared to 32 to the centralized system, a unified basis for comparison is obtained from extracting the diagonal elements from the full matrix and forming a new diagonal matrix.

As explained earlier, the elements of the new diagonal matrix have a great significance since they represent the symmetrical resistance of each power source with respect to the system centroid or reference point, and hence can serve as a justified basis for comparing more than one optimum power network in the sixth reference frame.

7. Results

Carrying out the procedure explained earlier for the establishment of the symmetrical resistance diagonal matrices for systems A and B, under all loading conditions, (P, = 60, 70, SO, 90 and 100% of peak load) the following information for 70% base loading is listed as a typical case for other loadings mentioned above.

Table **1** contains the diagonal elements of the [R] matrix for the 32 busbar centralized system extracted from the overall much larger [R] matrix.

Table 2 contains the diagonal elements of the [R] matrix for the 132 busbar dispersed-centralized system extracted from the much larger overall [R] matrix.

(continued on p. 152)

TABLE 1

Self-symmetric resistance matrix for centralized system
Values listed are 10^6 times their true p.u. values

Bus No.	70% Loading	Bus. No	70% Loading
1	73.9802	17	613880.3
2	1.3380	18	—69.4038
3	—396.5701	19	80.3259
4	62.0394	20	38.4445
5	8.5583	21	98.2755
6	—22.0731	22	429.6367
7	149.2670	23	3078.50
8	—14.2234	24	—38.7570
9	—7.1399	25	41.4405
10	—303.6730	26	29.4890
11	—3961.8000	27	0.7789
12	11.7583	28	29.4290
13	64.4223	29	3.7398
14	299.5341	30	267.4327
15	—255.2030	31	—95.4486
16	18.3579	32	736.7194

TABLE 2

Self-symmetric resistance matrix for dispersed-centralized system
Values listed are 10^6 times their true p.u.

Bus No.	70% Loading	Bus No.	70% Loading	Bus No.	70% Loading
1	58.1807	45	0.000	39	5.4057
2	0.0000	46	0.000	40	−0.3814
3	0.0000	47	0.000	41	0.0000
4	0.0000	48	0.123	42	0.0000
5	0.0000	49	0.000	43	0.0000
6	0.0000	50	0.000	44	0.0000
7	333.7475	51	0.000	45	0.0000
8	−24.7995	52	0.000	46	0.0000
9	0.0000	53	0.000	47	0.0000
10	0.0000	54	0.000	48	0.0000
11	0.0000	55	0.000	49	0.0000
12	61.8234	56	75.496	50	0.0000
13	0.0000	57	37.897	51	0.0000
14	0.0000	58	0.000	52	0.0000
15	0.0000	59	9.100	53	0.0000
16	0.0000	60	34.802	54	0.0000
17	14.9525	61	0.000	55	0.0000
18	0.6518	62	0.000	56	0.0000
19	0.0000	63	0.000	57	0.0000

20	0.0000	64	0.0000	108	0.0000
21	0.0000	65	3.8601	109	0.0000
22	0.0000	66	0.0000	110	0.0000
23	0.0000	67	5.1711	111	0.0000
24	0.0000	68	0.0000	112	0.0000
25	0.0000	69	0.0000	113	0.0000
26	0.0000	70	0.0000	114	0.0000
27	0.0000	71	0.0000	115	0.0000
28	0.0000	72	0.0000	116	0.0000
29	0.0000	73	−0.5968	117	0.0000
30	0.0000	74	−83.9000	118	0.0000
31	0.0000	75	0.0000	119	0.0000
32	0.0000	76	0.0000	120	0.0000
33	0.0000	77	0.0000	121	1.6660
34	0.0000	78	0.0000	122	0.0000
35	0.0000	79	0.0000	123	7.0156
36	0.0000	80	−339.6110		
37	0.0000	81	0.0000		
38	−8.3863	82	0.0000		
39	0.0000	83	0.0000		
40	0.0000	84	0.0000		
41	0.0000	85	0.0000		
42	0.0000	86	0.0000		
43	0.0000	87	0.0000		
44	1.3834	88	0.0000		

The diagonal elements listed in Tables 1 and 2 represent the elemental resistance path from each busbar in the power flow reference frame to the system centroid.

The finite elemental values indicated in Table 1 identify the presumed centralized mode of this system.

In Table 2, the elemental non-zero values refer to those power busbars of centralized location maintained in the new system with respect to total load supplied by them, while the zero elemental values refer to those dispersed busbars scattered in the power system at close proximity to the system centroid rendering their resistance path negligible as demonstrated by their zero values.

8. Conclusions

Economic evaluation, stability, reliability and the overall power system security, can be given direct and prompt analysis once the load flow calculation and optimum transmission loss coefficients information obtained for several power system alternatives, are established on different grounds.

This paper can support the following conclusions:

(a) Optimal form for the transmission loss coefficients matrix as expressed in eqn. (21) could be calculated at any fixed percentage of received load P_r, in terms of optimum capacities of all power sources and fuel cost data. Computer time required for obtaining the $[B]$ matrix from this method is much less than that needed for using the conventional form of the [B] matrix which depends on information derived from load flow calculations, such as voltage magnitude, phase angle, real and reactive power of all busbars, besides the power network constants.

(*b*) An overall $[R]$ matrix for an optimum power system reflecting network design in the power flow reference frame can be established for all loadings, based on data compiled from load flow calculations and optimum $[B]$ matrices.

(c) A diagonal $[R]$ matrix can be extracted from the overall matrix, to indicate on a smaller scale, (especially in a power system with large numbers of busbars) the direct resistive elemental path from each power equivalent busbar to the system centroid.

(d) Inspection of the order of magnitudes of the diagonal matrices under all percentages of total received loads for each optimum system can serve as a basic criterion for identifying that arbitrary interconnecting network and its eventual design in the actual reference frame.

Therefore, an inspection of Table 1, which lists the elements of diagonal matrices for an optimum centralized power system, under all percentages of loading, reveals that ail of those elements are non-zero and of sizeable values. This implies the feasibility of the optimal form of this centralized system, and consequently its design in the first reference frame.

Also, inspection of Table 2 indicates that all the newly established

dispersed power busbars have a zero resistance path with respect to the system reference point, while those non-zero values of the diagonal matrices refer to the originally existing centralized busbars. Hence this represents again the exact identification and feasibility of the presumed arbitrary interconnecting network for a disperseti-centralized power system and its design and physical r alization in the first frame.

The above procedure of network identification and its physical realization for the two optimum systems A and B, in fact serves as an example in comparing several power system alternative having different numbers of busbars, to be established under different constraints, as mentioned in the introductory part of this paper.

(e) Identification of a power system in the sixth reference frame (known as the power flow frame) can lead to system representation in each of the other preceding five frames, by applying the corresponding transformation matrices given by Kron. In the case of actual optimum power system design, its identification in the first reference frame (individual currents and actual interconnection) represents the direct operational form.

(f) Analyzing any power system in the power flow reference frame, can he very economical with respect to computer time and memory, since in this frame there will be a smaller total number of busbars and a smaller number of interconnecting branches.

Acknowledgement

The author wishes to thank the Middle Atlantic Power Research Committee for their support in sponsoring the research work presented in this paper.

References

1 J.F. Boshier, Economic operation for electric power systems, IEE, Electronics and Power, (1974) 418.

2 K.I. Denno, Power system synthesis from solution of optimum transmission loss coefficients, Conference paper C73462-9, presented at the IEEE, PES Summer Meeting in Vancouver, Canada, July 1973.

3 L.K. Kirchmayer, Economic Operation of Power Systems, John Wiley & Sons, Inc., New York, 1958.

4 G. Kron, Tensorial analysis of integrated transmission systems, AIEE Trans. Power Syst. and Appar., 70 (1951) 1239.

5 G.W. Stagg and A.H. El—Abiad, Computer Methods in Power System Analysis, McGraw-Hill Book Company, New York, 1968.

Journal of Applied Science and Engineering A, 2 (1977) 155

Letter to the Editor

Van der Pol's problem is essentially one of those requiring the — holophysical — Aristomodel for its solution.

A projection of this space model is given in the Figure; it may be compared to the circuitry used by Tellegen in his gyrator, wherein an inductance in the metallic part of the circuit I converts into a capacitance in circuit II, the circuits being coupled in a plasma p, in which I suffers attenuation (+) thereby (microphysically) inducing (negative) attenuation in circuit II. Besides the plasma conversion of L into C is also active in the inversion of + into — for the attenuation it introduces; the usual Barkhausen approximations cannot be used, nor may understanding of this phenomenon be furthered by macro-considerations (the negative resistance in II inducing oscillations in its own resonances). The negative damping mentioned in line 4 of J.W. Alexander's article (Vol. **1,** No. 4) cannot otherwise be found. Apart from this remark his calculations are of course beyond question.

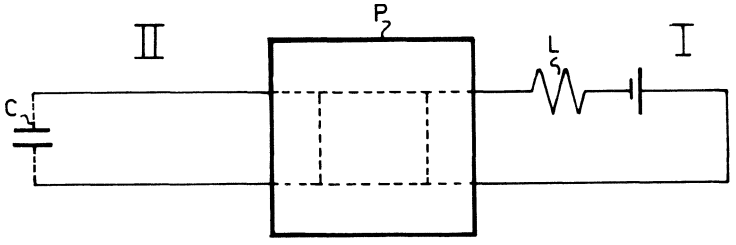

A more detailed account of Holophysics and its relation to Economics and to the 5 Disciplines treated for Unsolved Riddles, discussed at the 27th Sept. conference of the Natuur- en Geneeskundig Congres in Amsterdam (1975) may be found in the contribution to ZWO at the Hague (Korteweg and Wynma, unpublished paper). Plasmap may be taken as a Neon tube, circuit I as its power, II as its parallel capacitance. For a comparable introduction to negative friction see also Morse and Fresbach, Methods of Theoretical Physics, McGraw-Hill, N.Y., 1953, Vol. I, p. 298.

L.A.W. van der Lek
Oud Ade (The Netherlands)

Submission of papers

Papers should be submitted to the Technical Editor: Ir. M. Skaliks, Twente University of Technology, Postbox 217, Enschede, The Netherlands.

Manuscript preparation

Three copies of the manuscript should be submitted in double-spaced typing on pages of uniform size with a wide margin on the left. The top copy should bear the name and full postal address of the person to whom proofs are to be sent. A summary of 100--200 words is required.

References should be numbered consecutively throughout the text and collected together in a reference list at the end of the paper. Journal titles should be abbreviated. The abbreviated title should be followed by volume number, year (in parentheses), and page number.

Illustrations

Line drawings should be in a form suitable for reproduction, drawn in Indian ink on drawing paper. They should preferably all require the same degree of reduction, and should be submitted on paper of the same size, or smaller than, the main text, to prevent damage in transit. Photographs should be submitted as clear black-and-white prints on glossy paper. Each illustration must be clearly numbered.

Legends to the illustrations must be submitted in a separate list.

All tables and illustrations should be numbered consecutively and separately throughout the paper.

Language

The language of the Journal is English.

Proofs

Authors will receive galley proofs, which they are requested to correct and return as soon as possible. No new material may be inserted in the text at the time of proofreading.

Reprints

A total of 50 reprints of each paper will be supplied free of charge to the author(s). Additional copies can be ordered at prices shown on the reprint order form which accompanies the galley proofs.

Subscription information

Quarterly publication. Four issues per volume. Subscription price: Dfl. 141.00 (approx. US $ 56) per volume plus postage Dfl. 14.00.
Subscribers in the U.S.A. and Canada receive their copies by airmail. A specimen copy will be sent on request. For advertising rates apply to the publishers.
Subscription orders should be sent to: Elsevier Scientific Publishing Company, P.O. Box 211, Amsterdam, The Netherlands.
Claims for issues not received should be made within three months of publication of the issues. If not, they cannot be honoured free of charge.

A pamphlet containing more detailed instructions on the preparation of manuscripts for the JOURNAL OF APPLIED SCIENCE AND ENGINEERING. SECTION A may be obtained from the publishers

VOL. 2, No. 2. JUNE 1977

JOURNAL OF APPLIED SCIENCE AND ENGINEERING
SECTION A: ELECTRICAL POWER AND INFORMATION SYSTEMS

CONTENTS

Printed in The Netherlands